Satellite Orbit Determination

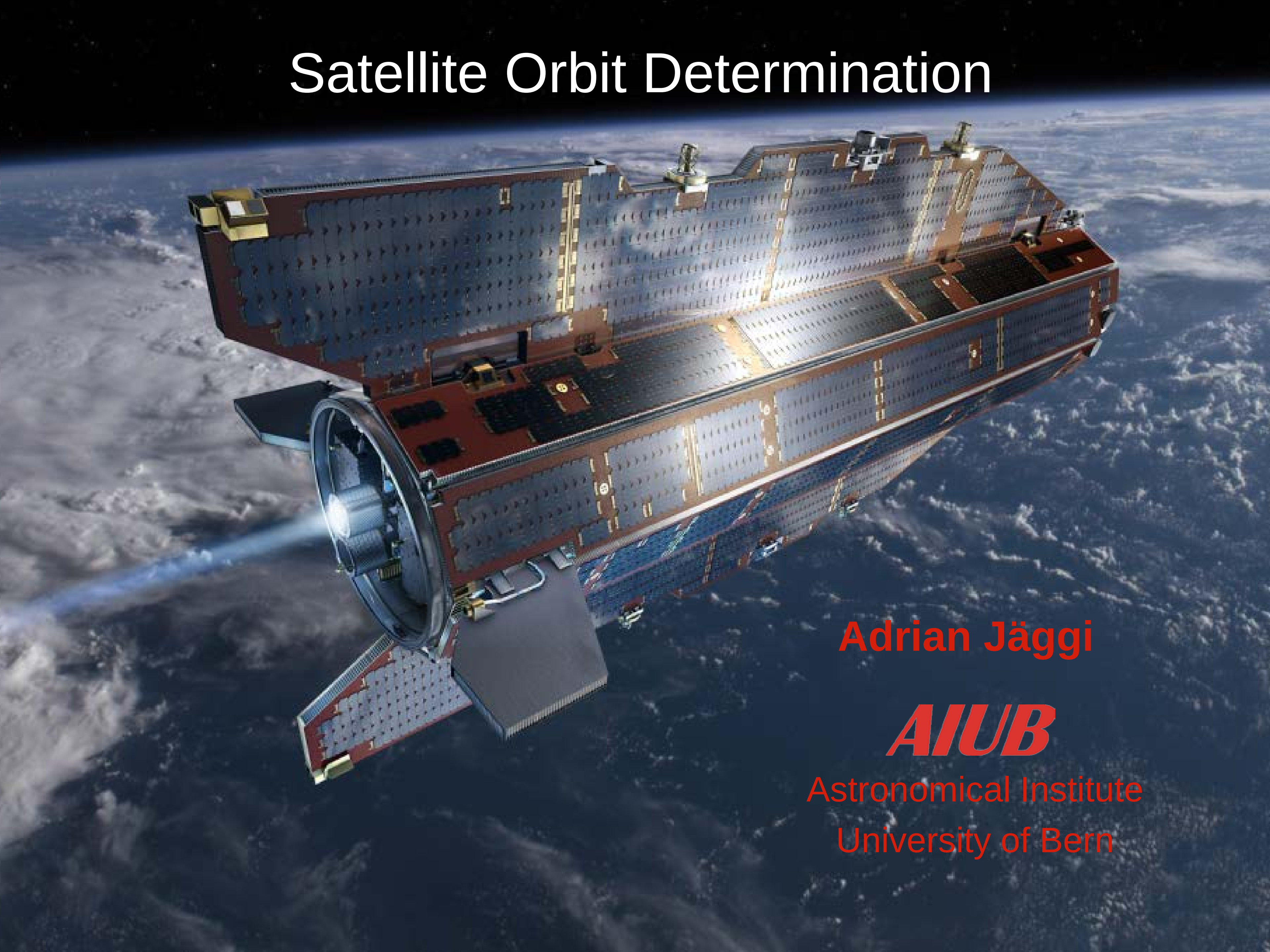

Adrian Jäggi

AIUB

Astronomical Institute
University of Bern

Low Earth Orbiters (LEOs)

GRACE

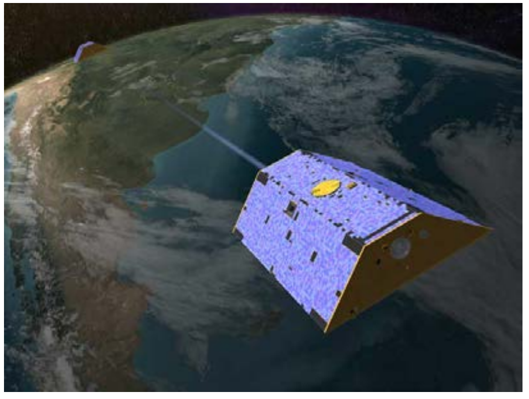

Gravity **R**ecovery **A**nd **C**limate **E**xperiment

GOCE

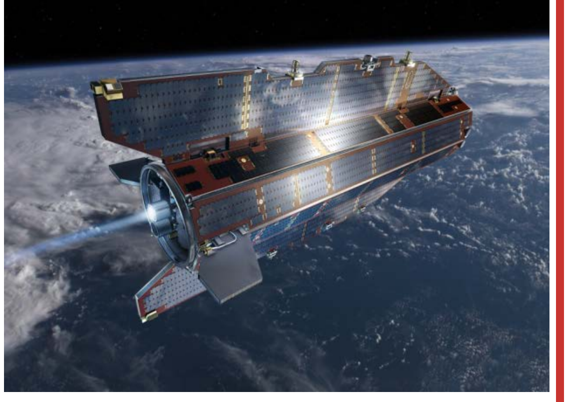

Gravity and steady-state **O**cean **C**irculation **E**xplorer

TanDEM-X

TerraSAR-X **a**dd-o**n** for **D**igital **E**levation **M**easurement

Of course, there are many more missions equipped with GPS receivers

Jason

Jason-2

MetOp-A

Icesat

COSMIC

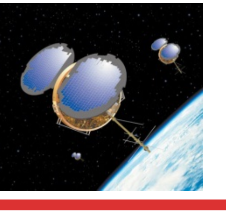

LEO Orbit Characteristics – the example of GOCE

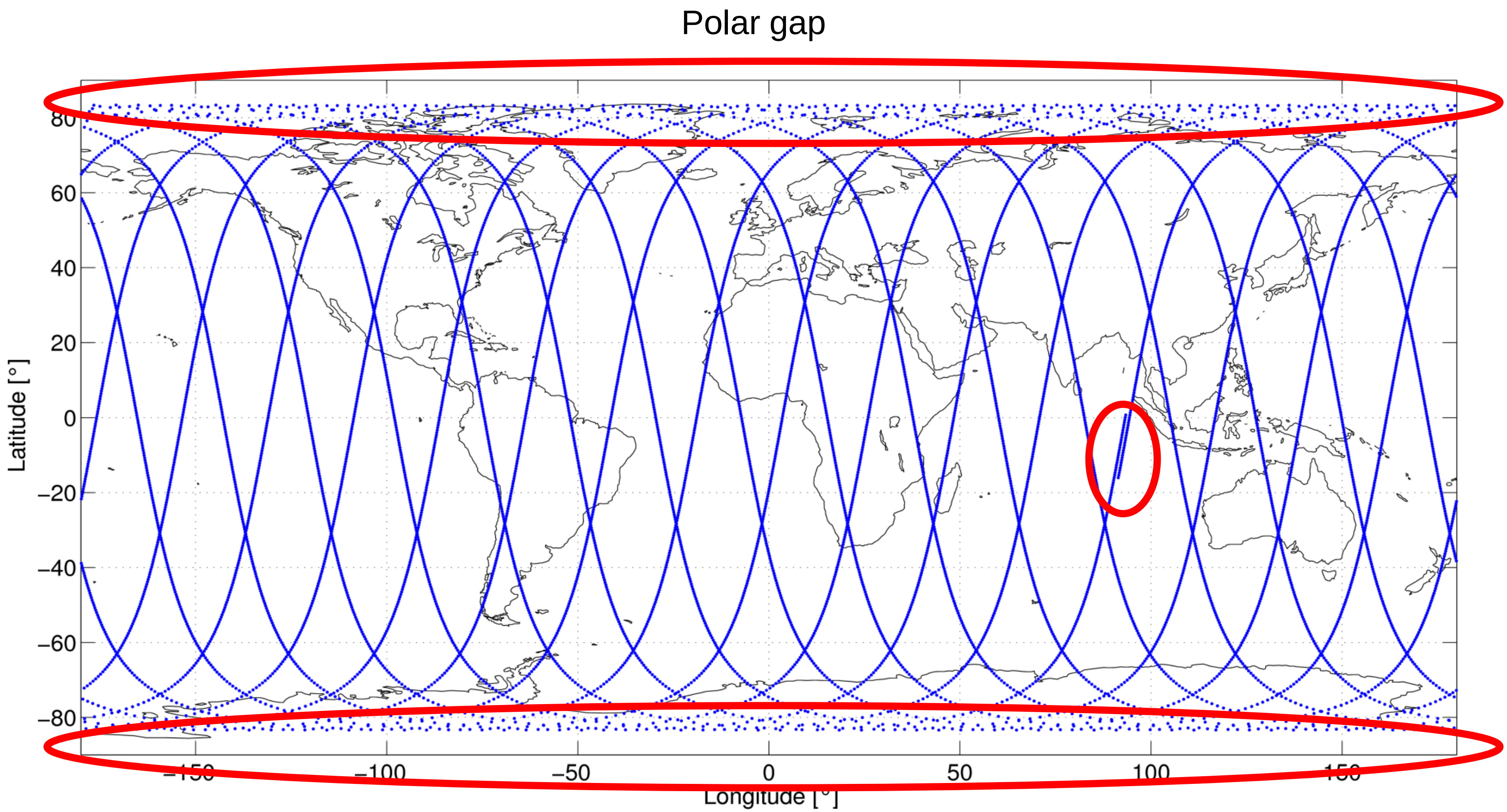

Ground-track coverage on 2 Nov, 2009
Dusk-dawn sun-synchronous orbit (i = 96.6°)

Complete geographical coverage after 979 revolutions (repeat-cycle of 61 days)

Introduction to GPS

GPS: **G**lobal **P**ositioning **S**ystem

Characteristics:

- Satellite system for (real-time) **Positioning** and **Navigation**
- **Global** (everywhere on Earth, up to altitudes of 5000km) and **at any time**
- **Unlimited** number of users
- **Weather-independent** (radio signals are passing through the atmosphere)
- **3-dimensional position**, **velocity** and **time** information

GPS Segments

The GPS consists of **3 main segments**:

- **Space Segment**: the satellites and the constellation of satellites
- **Control Segment**: the ground stations, infrastructure and software for operation and monitoring of the GPS
- **User Segment**: all GPS receivers worldwide and the corresponding processing software

We should add an important **4th segment**:

- **Ground Segment**: all civilian permanent networks of reference sites and the international/regional/local services delivering products for the users

Space Segment

- The space segment nominally consists of **24 satellites**, presently: **32** active GPS satellites

- Constellation design: at least **4 satellites** in view from **any location** on the Earth at **any time**

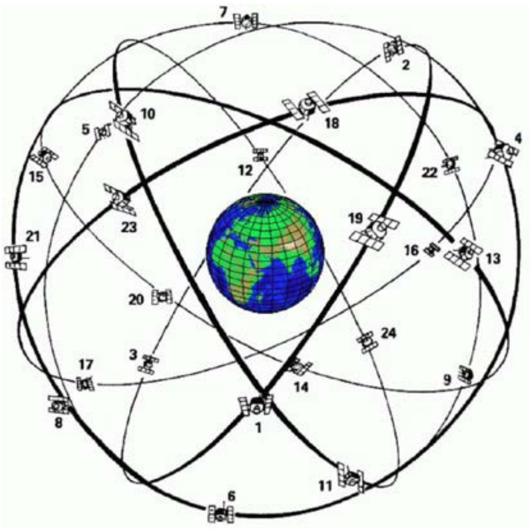

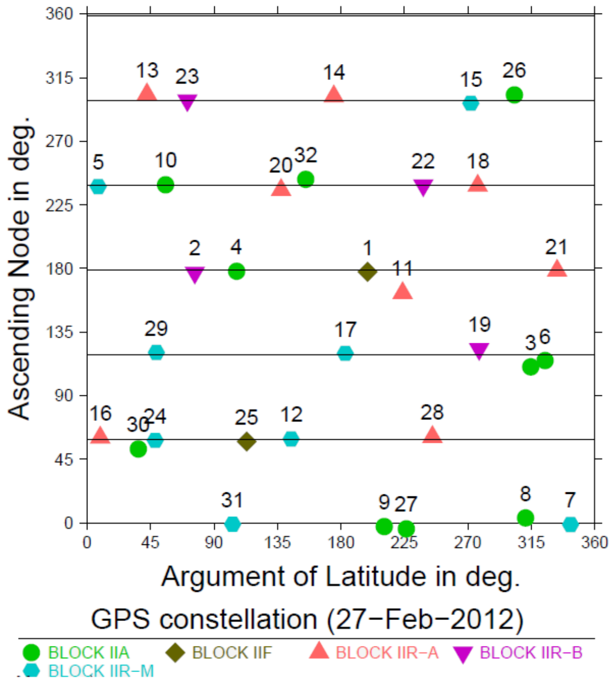

Control Segment

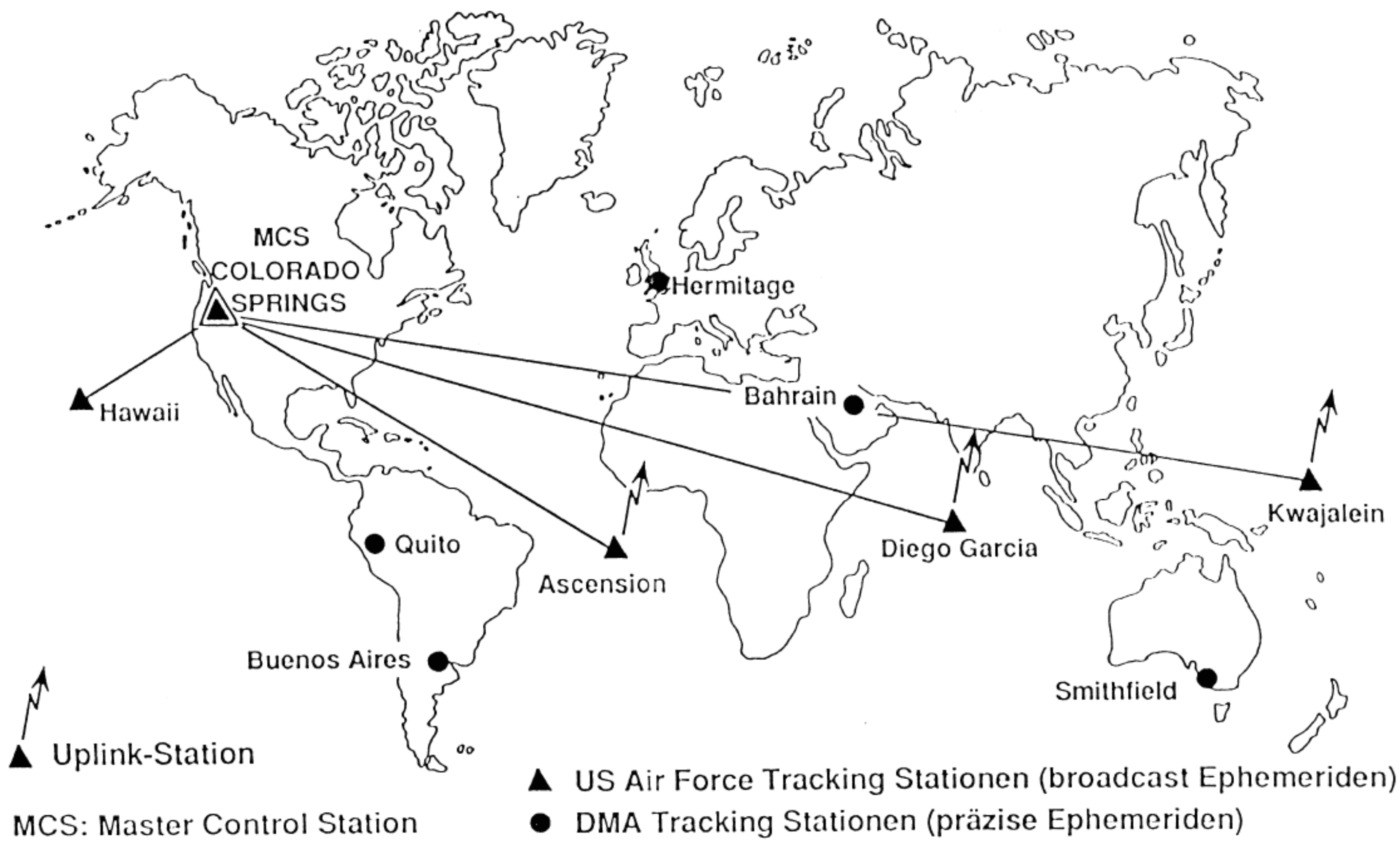

User Segment and Ground Segment

User Segment:

- All **GPS receivers** on land, on sea, in the air and in space
- Broad user community with applications of the GPS for positioning and navigation, surveying, geodynamics and geophysics, atmosphere, …

Ground Segment:

- Global network of the International GNSS Service (IGS: ~ 400 stations)
- Regional and local permanent networks (Europe, Japan, US): densification of the reference frame, positioning services

Global Network of the IGS

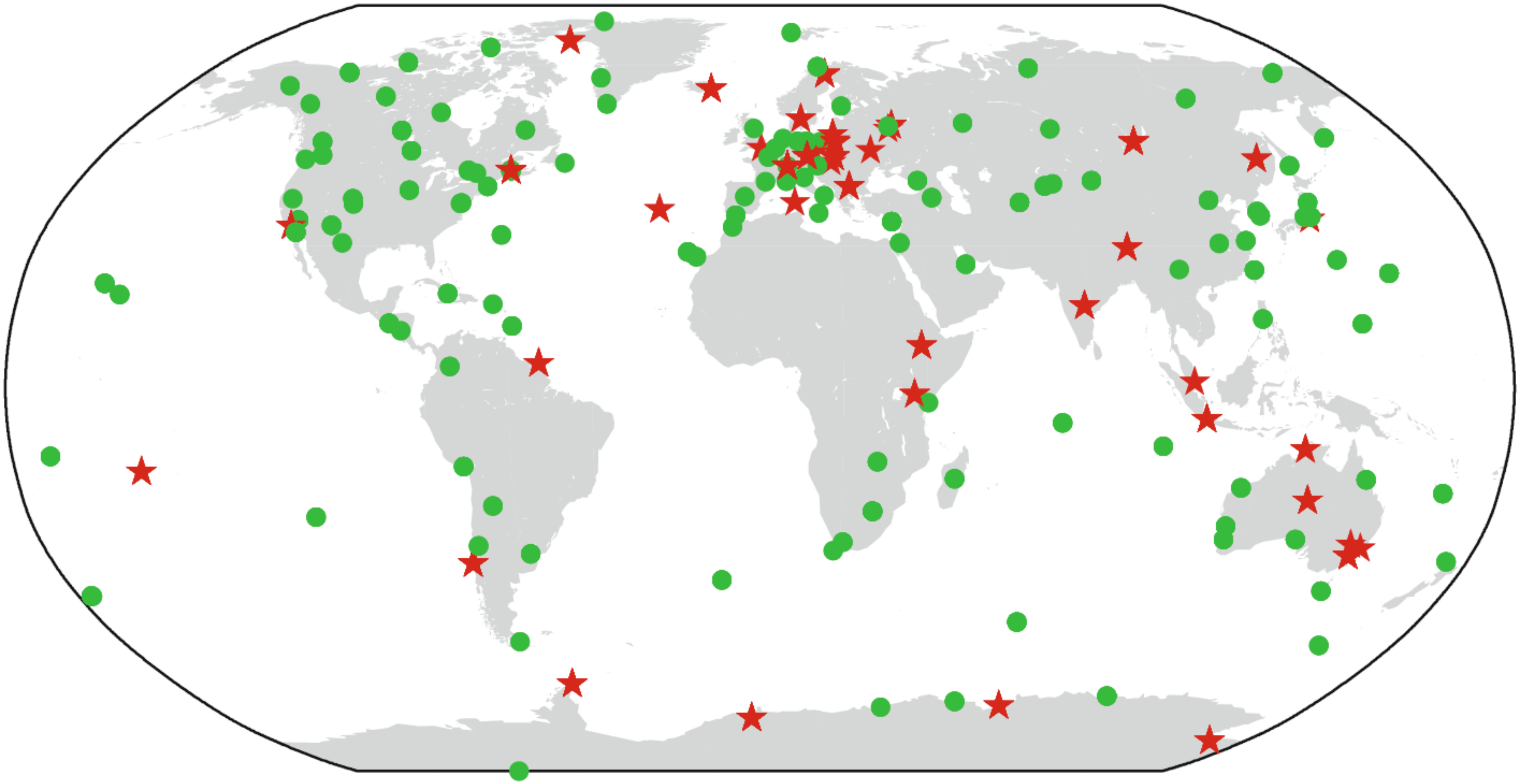

● GPS-only receivers

★ Combined GPS-GLONASS receivers

IGS stations used for computation of final orbits at CODE (Dach et al., 2009)

Global Network of the IGS

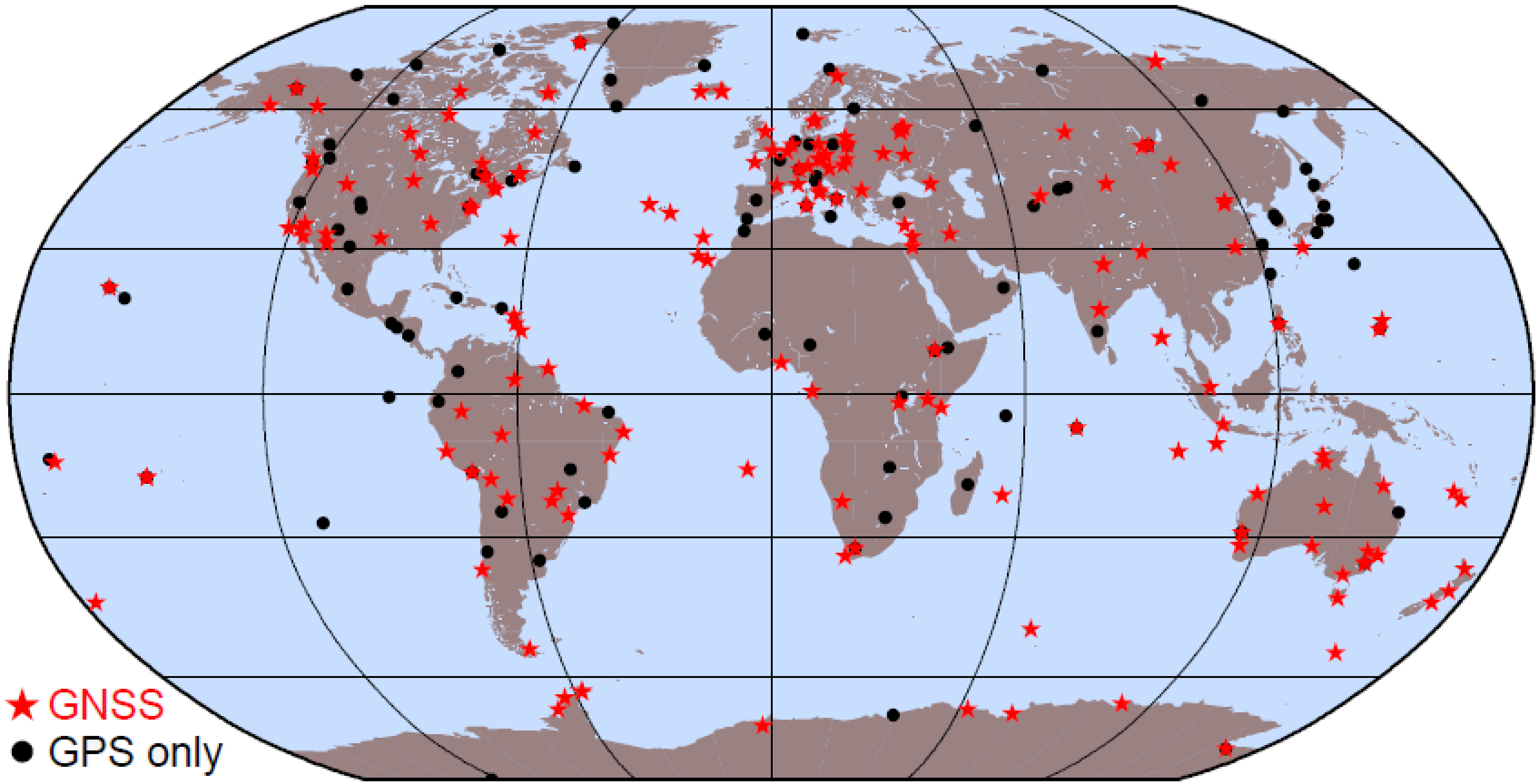

More and more multi-GNSS receivers are available in the global network of the IGS

IGS stations used for computation of final orbits at CODE (November 2011)

Main components of the IGS

- **Regional and Global Data Centers**
  provide the data to the users and analysis centers
- **Analysis Centers**
  compute the products from the data of the IGS–stations
- **Analysis Center Coordinator**
  combines the contributions from the analysis centers to IGS–products
- **Product Databases**
  provide the IGS products to the users
- **IGS Central Bureau**
  day-to-day management of the IGS
- **IGS Governing Board**
  policy guidance of the IGS

Analysis Centers (ACs) of the IGS

CODE (Center for Orbit Determination in Europe) as an example:

CODE is a joint-venture between:

- Astronomical Institute of the University of Bern (AIUB), Bern, Switzerland
- Swiss Federal Office of Topography (swisstopo), Wabern, Switzerland
- German Federal Office for Cartography and Geodesy (BKG), Frankfurt, Germany
- Institute of Astronomical and Physical Geodesy (IAPG) of the Technische Universität München (TUM), Munich, Germany

AIUB

Schweizerische Eidgenossenschaft
Confédération suisse
Confederazione Svizzera
Confederaziun svizra

Bundesamt für
Kartographie und Geodäsie

TUM
Technische Universität München

Products of the IGS

Series	Product Type	Accuracy	
Ultra-Rapid (predicted)	GNSS Orbits GPS satellite clocks EOPs	GPS: 5 cm (1D) RMS: 3 ns PM: 250 µas	GLONASS: 10 cm (1D) SDev: 1.5 ns dLOD: 50 µs
Ultra-Rapid (observed)	GNSS Orbits GPS satellite clocks EOPs	GPS: 3 cm (1D) RMS: 150 ps PM: <150 µas	GLONASS: 10 cm (1D) SDev: 50 ps dLOD: 10 µs
Rapid	GNSS Orbits GPS sat. & rec. clocks EOPs	GPS: 2.5 cm (1D) RMS: 75 ps PM: <40 µas	SDev: 25 ps dLOD: 10 µs
Final	GNSS Orbits GPS sat. & rec. clocks EOPs Terrestrial Frame	GPS: 2.5 cm (1D) RMS: 75 ps PM: <30 µas N&E: 2 mm	GLONASS: <5 cm (1D) SDev: 20 ps dLOD: 10 µs U: 5 mm

Computation of Final Orbits at CODE

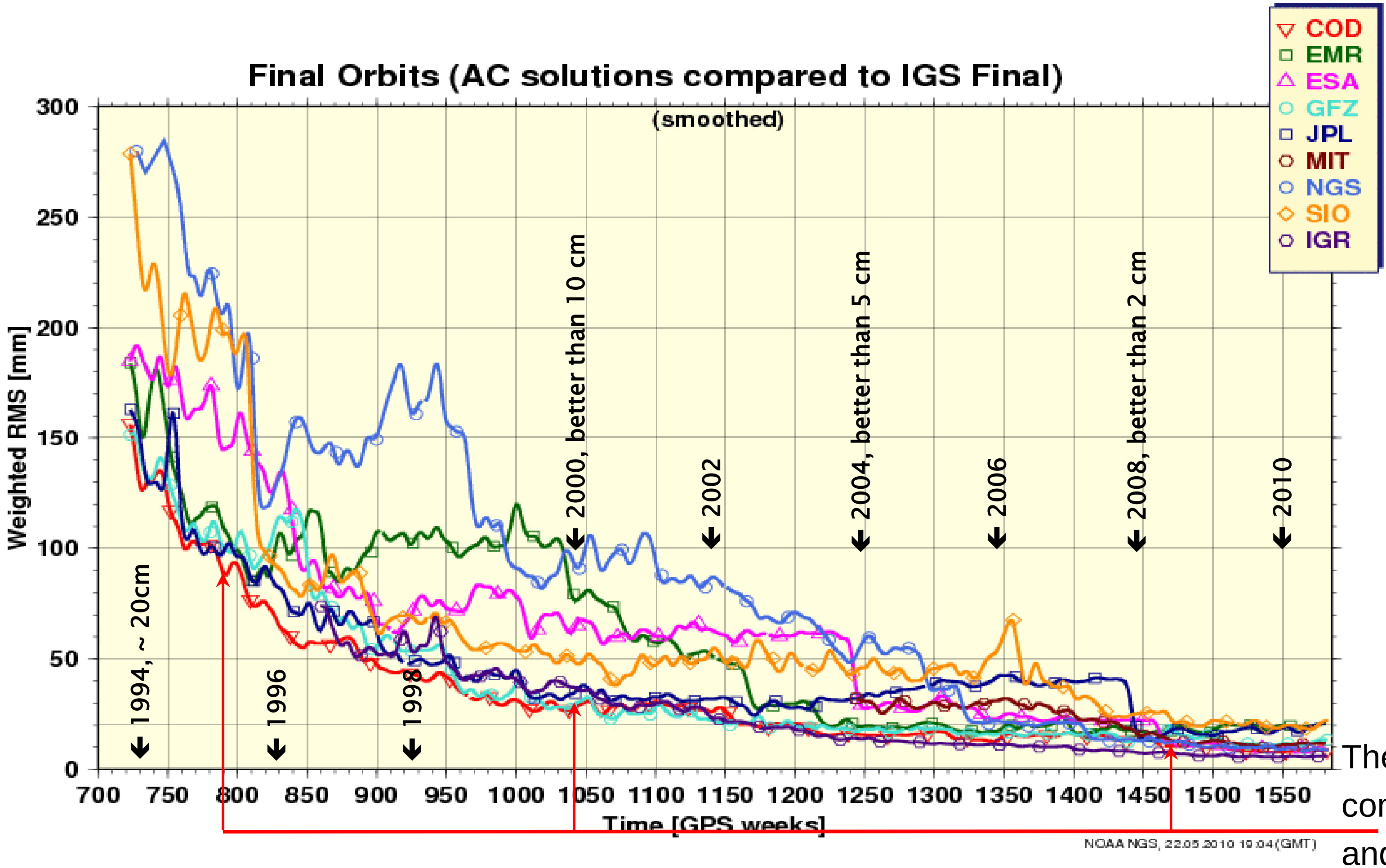

The COD solution is computed at AIUB and used for GOCE orbit determination

Computation of Final Orbits at CODE

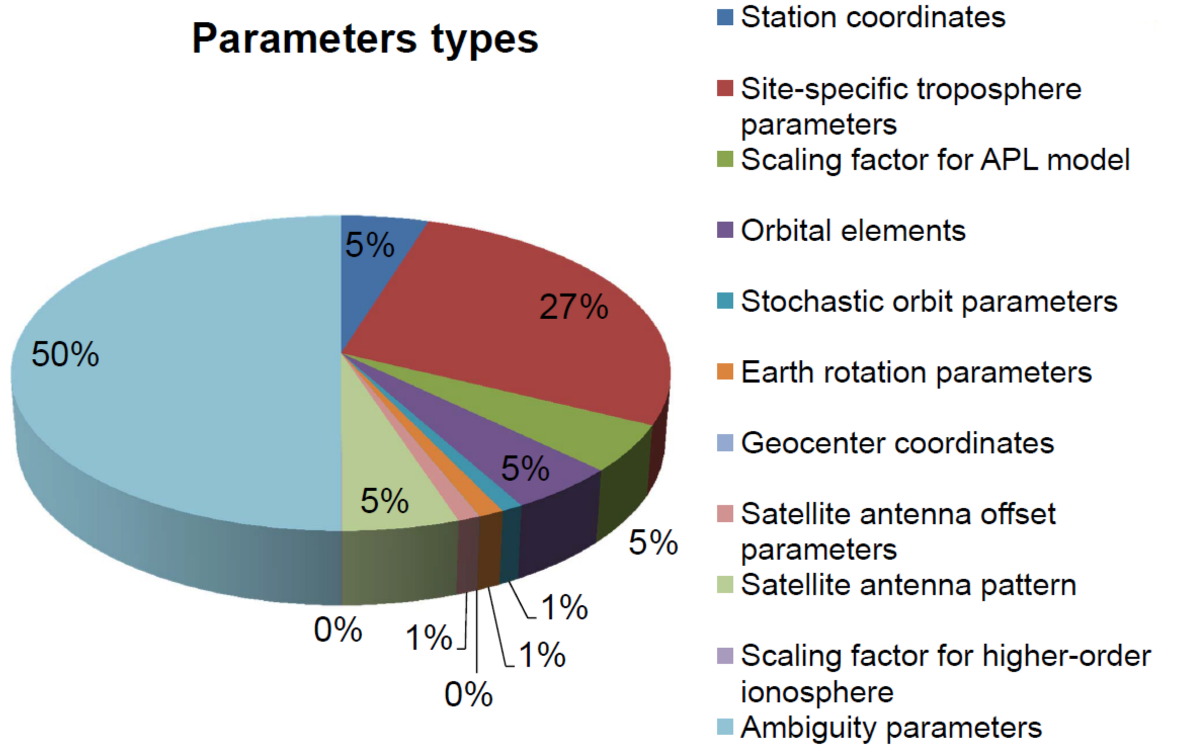

A large number of parameters has to be **co-estimated** together with the orbital parameters, such as …

Computation of Final Orbits at CODE

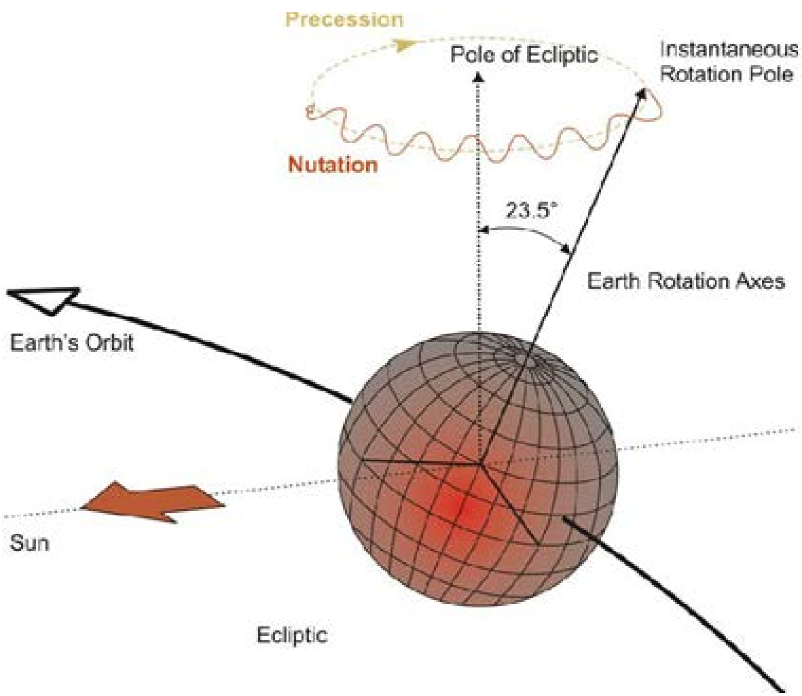

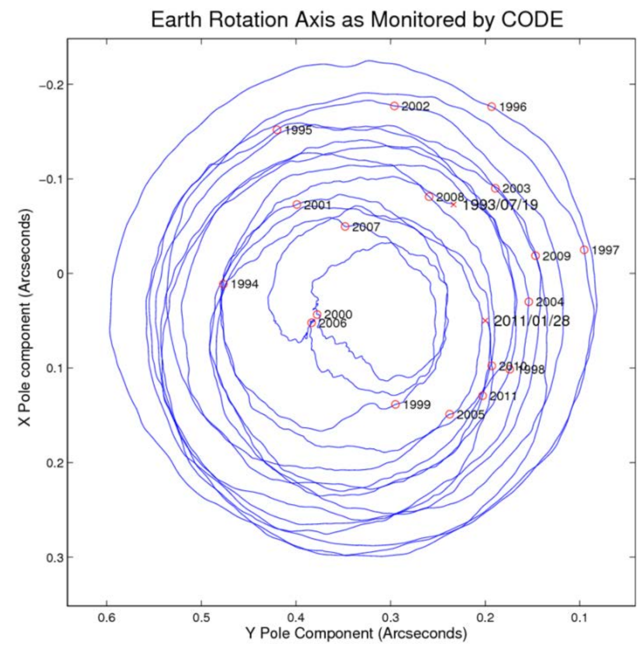

… Earth Rotation Parameters (ERP). They define the transformation between the inertial reference frame (ICRF) and the terrestrial reference frame (ITRF) as

$$\boldsymbol{r}_{ITRF} = \boldsymbol{X}^T \boldsymbol{Y}^T \boldsymbol{U} \boldsymbol{N} \boldsymbol{P} \boldsymbol{r}_{ICRF}$$

Computation of Final Clocks at CODE

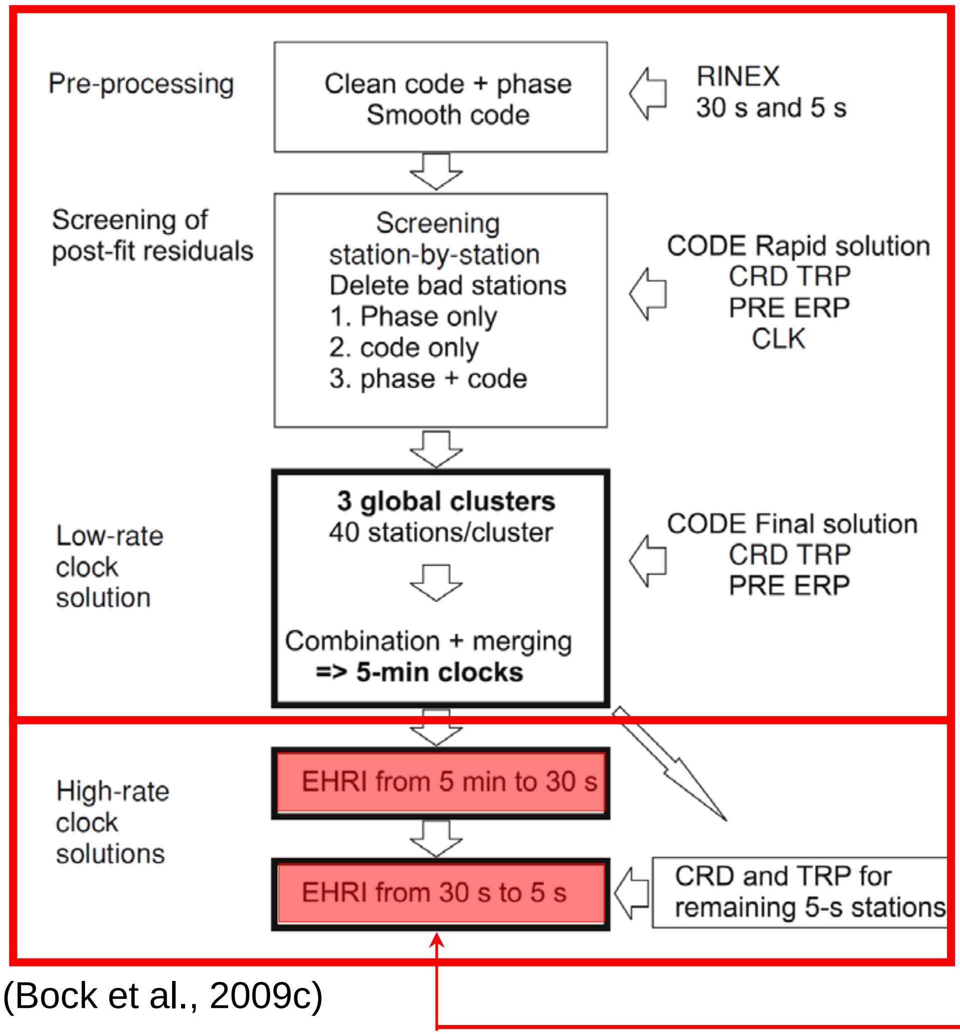

(Bock et al., 2009c)

The final clock product with 5 min sampling is based on undifferenced GPS data of the IGS network

The IGS 1 Hz network is finally used for clock densification to 5 sec

The 5 sec clocks are interpolated to 1 sec as needed for GOCE orbit determination

Computation of (Near) Real Time Clocks

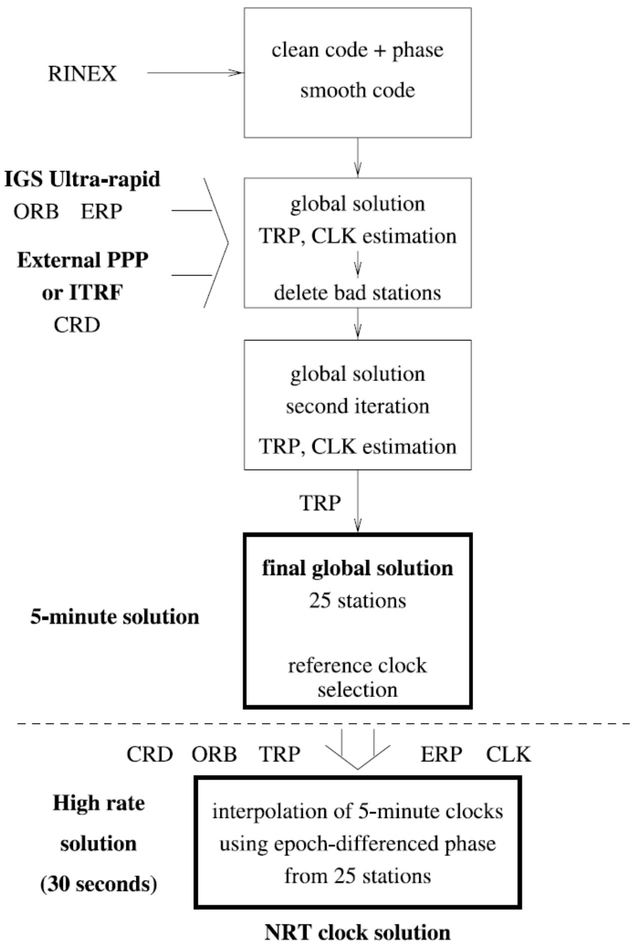

(Bock et al., 2009a)

Similar procedures can be adopted for the NRT clock computation as for the final clock computation. The availability of real-time data streams is crucial

Real time clock estimation procedures are described in (Hauschild and Montenbruck, 2008)

GPS Signals

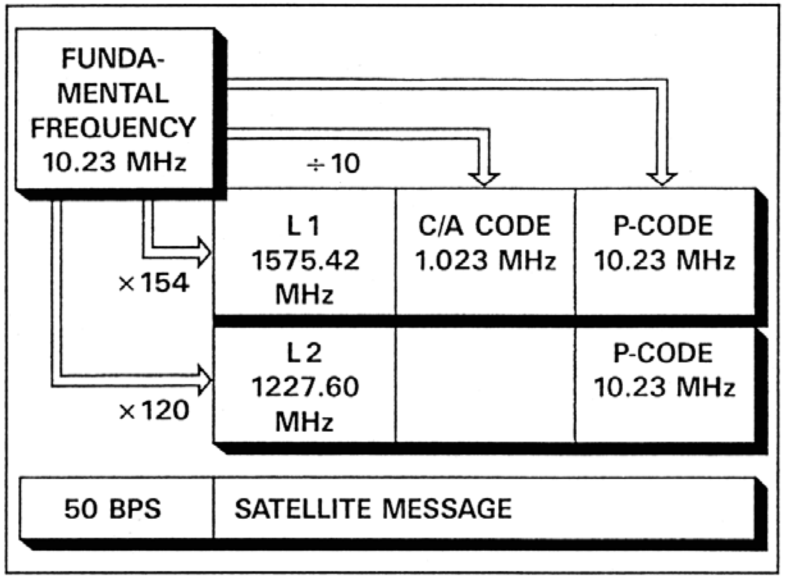

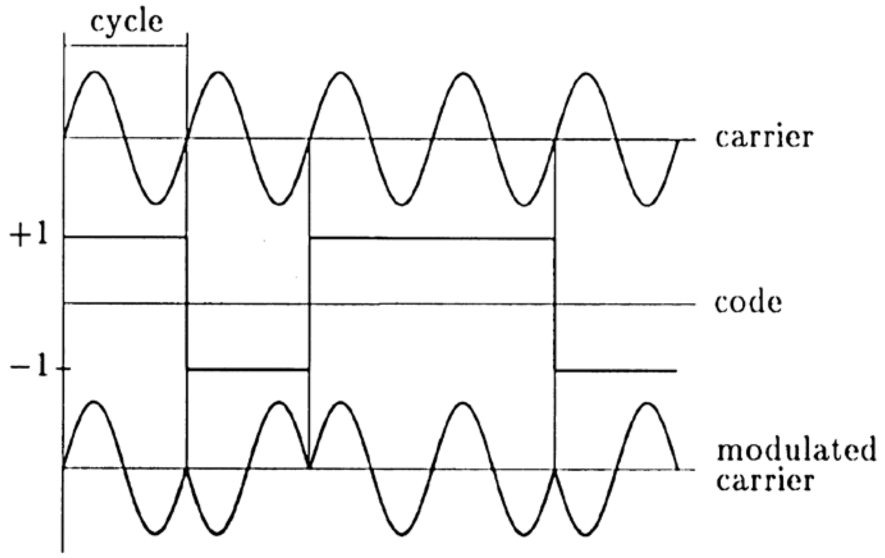

Signals driven by an **atomic clock**

Two **carrier signals** (sine waves):

- **L1**: f = 1575.43 MHz, λ = 19 cm
- **L2**: f = 1227.60 MHz, λ = 24 cm

Bits encoded on carrier by phase modulation:

- **C/A-code** (Clear Access / Coarse Acquisition)
- **P-code** (Protected / Precise)
- **Broadcast/Navigation Message**

Pseudorange / Code Measurements

Code Observations P_i^k are defined as:

$$P_i^k \doteq c\,(T_i - T^k)$$

c Spee

T_i Recei

T^k GPS ne)

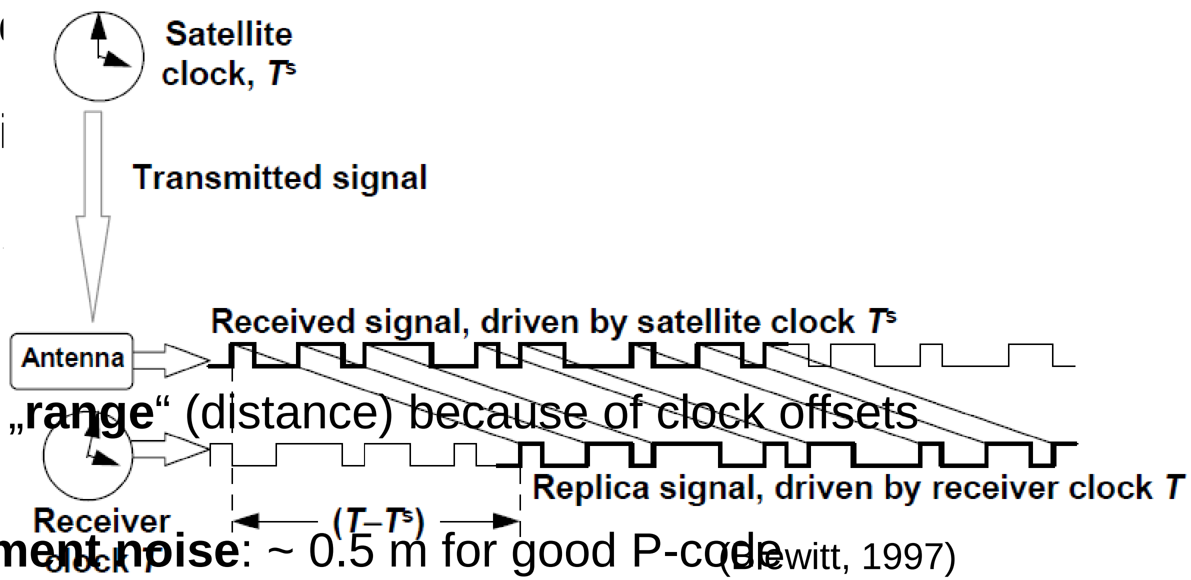

(Blewitt, 1997)

- No actual „**range**“ (distance) because of clock offsets
- **Measurement noise**: ~ 0.5 m for good P-code

Code Observation Equation

$$P_i^k = \rho_i^k - c \cdot \Delta t^k + c \cdot \Delta t_i$$

t_i, t^k GPS time of reception and emission

Δt^k Satellite clock offset $T^k - t^k$

Δt_i Receiver clock offset $T_i - t_i$

ρ_i^k Distance between receiver and satellite $c\,(t_i - t^k)$

Known from ACs or IGS:

- satellite positions $(x^{k_j}, y^{k_j}, z^{k_j})$
- satellite clock offsets Δt^{k_j}

4 unknown parameters:

- receiver position (x_i, y_i, z_i)
- receiver clock offset Δt_i

Basic Positioning and Navigation Concept (1)

Simplified model for ρ_i^k: atmospheric delay missing, exactly 4 satellites, …

$$P_i^{k_1} = \sqrt{(x^{k_1} - x_i)^2 + (y^{k_1} - y_i)^2 + (z^{k_1} - z_i)^2} - c \cdot \Delta t^{k_1} + c \cdot \Delta t_i$$

$$P_i^{k_2} = \sqrt{(x^{k_2} - x_i)^2 + (y^{k_2} - y_i)^2 + (z^{k_2} - z_i)^2} - c \cdot \Delta t^{k_2} + c \cdot \Delta t_i$$

$$P_i^{k_3} = \sqrt{(x^{k_3} - x_i)^2 + (y^{k_3} - y_i)^2 + (z^{k_3} - z_i)^2} - c \cdot \Delta t^{k_3} + c \cdot \Delta t_i$$

$$P_i^{k_4} = \sqrt{(x^{k_4} - x_i)^2 + (y^{k_4} - y_i)^2 + (z^{k_4} - z_i)^2} - c \cdot \Delta t^{k_4} + c \cdot \Delta t_i$$

More than 4 satellites: best receiver position and clock offset with **least-squares** or **filter** algorithms

Basic Positioning and Navigation Concept (2)

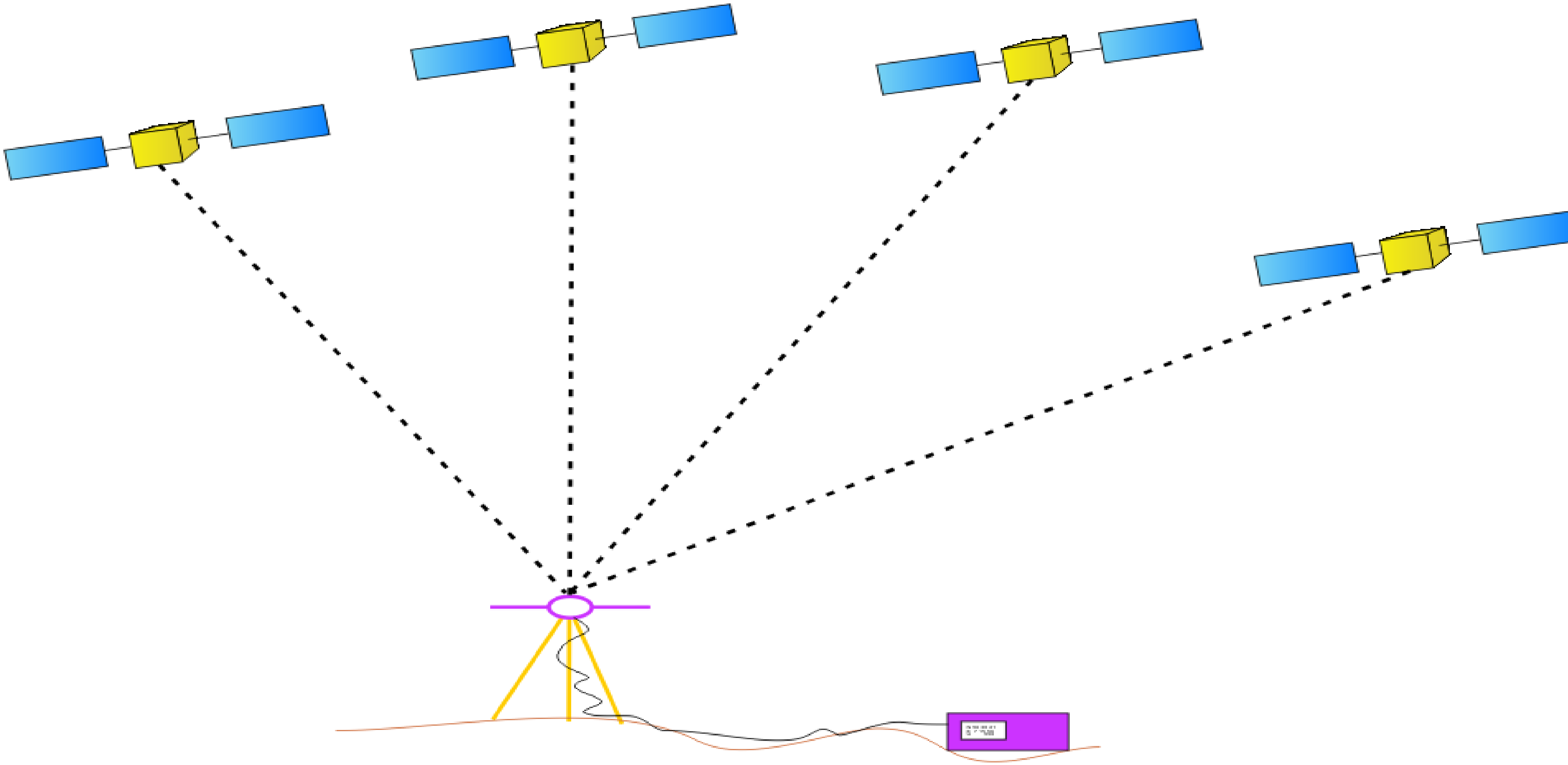

Carrier Phase Measurements (1)

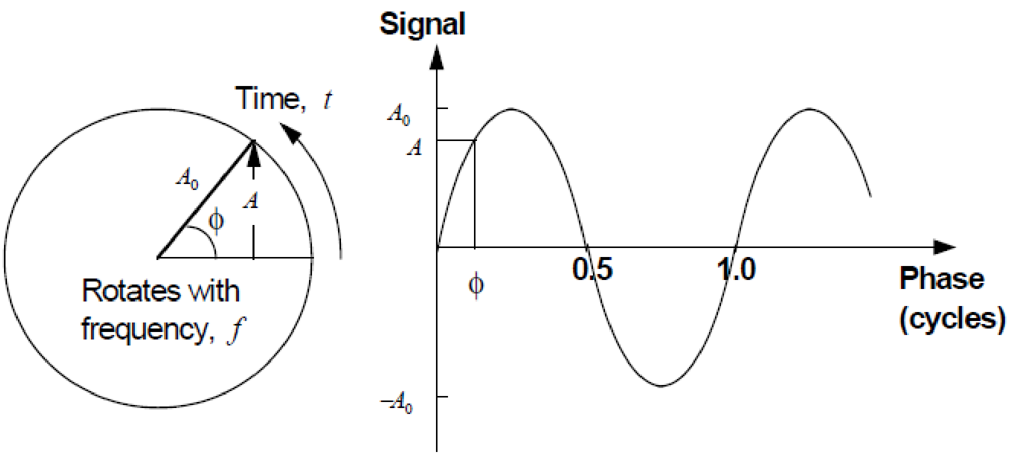

Phase ϕ (in cycles) increases linearly with time t :

$$\phi = f \cdot t$$

where f is the frequency

The **satellite** generates with its clock the phase signal ϕ^k. At emmision time T^k (in satellite clock time) we have

$$\phi^k = f \cdot T^k$$

The same phase signal, e.g., a wave crest, propagates from the satellite to the receiver, but the receiver measures only the fractional part of the phase and does not know the **integer number of cycles** N_i^k (phase ambiguity):

$$\phi_i^k = \phi^k - N_i^k = f \cdot T^k - N_i^k$$

Carrier Phase Measurements (2)

The **receiver** generates with its clock a **reference phase.** At time of reception T_i of the satellite phase ϕ_i^k (in receiver clock time) we have:

$$\phi_i = f \cdot T_i$$

The actual **phase measurement** is the difference between receiver reference phase ϕ_i and satellite phase ϕ_i^k:

$$\psi_i^k = \phi_i - \phi_i^k = f \cdot T_i - (f \cdot T^k - N_i^k) = f \cdot (T_i - T^k) + N_i^k$$

Multiplication with the wavelength $\lambda = c/f$ leads to the **phase observation equation** in meters:

$$\begin{aligned} L_i^k &= \lambda \cdot \psi_i^k = c \cdot (T_i - T^k) + \lambda \cdot N_i^k \\ &= \rho_i^k - c \cdot \Delta t^k + c \cdot \Delta t_i + \lambda \cdot N_i^k \end{aligned}$$

Difference to the pseudorange observation: **integer ambiguity term** N_i^k

Improved Observation Equation

$$L_i^k = \rho_i^k - c \cdot \Delta t^k + c \cdot \Delta t_i + \cancel{T_i^k} + \cancel{I_i^k} + \lambda \cdot N_i^k$$
$$+ \Delta_{rel} - c \cdot b^k + c \cdot b_i + m_i^k + \epsilon_i^k$$

ρ_i^k	Distance between satellite and receiver	←	Satellite positions and clocks
Δt^k	Satellite clock offset wrt GPS time	←	are known from ACs or IGS
Δt_i	Receiver clock offset wrt GPS time		
~~T_i^k~~	~~Tropospheric delay~~	←	Not existent for LEOs
~~I_i^k~~	~~Ionospheric delay~~	←	Cancels out (first order only) when forming the ionosphere-free linear combination:
N_i^k	Phase ambiguity		
Δ_{rel}	Relativistic corrections		
b^k	Delays in satellite (cables, electronics)		
b_i	Delays in receiver and antenna		
m_i^k	Multipath, scattering, bending effects		
ϵ_i^k	Measurement error		

$$L_c = \frac{f_1^2}{f_1^2 - f_2^2} L_1 - \frac{f_2^2}{f_1^2 - f_2^2} L_2$$

Geometric Distance

Geometric distance ρ_{leo}^k is given by:

$$\rho_{leo}^k = \left|\boldsymbol{r}_{leo}(t_{leo}) - \boldsymbol{r}^k(t_{leo} - \tau_{leo}^k)\right|$$

$\boldsymbol{r}_{leo}$ Inertial position of LEO antenna phase center at reception time

$\boldsymbol{r}^k$ Inertial position of GPS antenna phase center of satellite k at emission time

τ_{leo}^k Signal traveling time between the two phase center positions

Different ways to represent $\boldsymbol{r}_{leo}$:

- **Kinematic** orbit representation
- **Dynamic** or **reduced-dynamic** orbit representation

Kinematic Orbit Representation (1)

Satellite position $\boldsymbol{r}_{leo}(t_{leo})$ (in inertial frame) is given by:

$$\boldsymbol{r}_{leo}(t_{leo}) = \boldsymbol{R}(t_{leo}) \cdot (\boldsymbol{r}_{leo,e,0}(t_{leo}) + \delta\boldsymbol{r}_{leo,e,ant}(t_{leo}))$$

$\boldsymbol{R}$	Transformation matrix from Earth-fixed to inertial frame
$\boldsymbol{r}_{leo,e,0}$	LEO center of mass position in Earth-fixed frame
$\delta\boldsymbol{r}_{leo,e,ant}$	LEO antenna phase center offset in Earth-fixed frame

Kinematic positions $\boldsymbol{r}_{leo,e,0}$ are estimated for each **measurement epoch**:

- Measurement epochs **need not** to be identical with nominal epochs
- Positions are **independent** of models describing the LEO dynamics
  Velocities cannot be provided

Kinematic Orbit Representation (2)

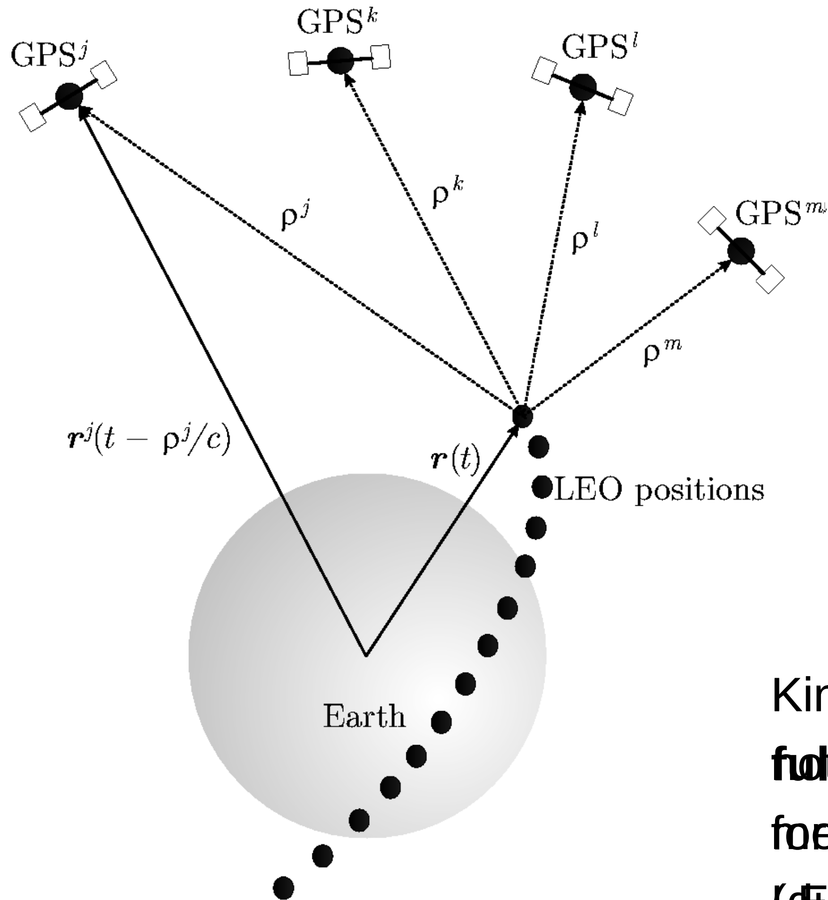

A kinematic orbit is an ephemeris at **discrete** measurement epochs

Kinematic positions are **fully independent** of the force models used for LEO orbit determination

Kinematic positions are not correlated if phase measurements are used (due to ambiguities)

(Svehla and Rothacher, 2004)

Kinematic Orbit Representation (3)

Measurement epochs (in GPS time)

Positions (km) (Earth-fixed)

```
*  2009 11  2  0  0  0.80678020
PL15  -390.612059   6623.987679     73.104149  193219.797196
*  2009 11  2  0  0  1.80678020
PL15  -389.240315   6624.166512     65.402457  193219.799413
*  2009 11  2  0  0  2.80678020
PL15  -387.868014   6624.336133     57.700679  193219.801634
*  2009 11  2  0  0  3.80678020
PL15  -386.495163   6624.496541     49.998817  193219.803855
*  2009 11  2  0  0  4.80678019
PL15  -385.121760   6624.647724     42.296889  193219.806059
*  2009 11  2  0  0  5.80678019
PL15  -383.747819   6624.789703     34.594896  193219.808280
*  2009 11  2  0  0  6.80678019
PL15  -382.373332   6624.922464     26.892861  193219.810495
*  2009 11  2  0  0  7.80678019
PL15  -380.998306   6625.046003     19.190792  193219.812692
*  2009 11  2  0  0  8.80678019
PL15  -379.622745   6625.160329     11.488692  193219.814899
*  2009 11  2  0  0  9.80678018
PL15  -378.246651   6625.265448      3.786580  193219.817123
```

Clock correction to nominal epoch (μs), e.g., to epoch 00:00:03

Excerpt of kinematic GOCE positions at begin of 2 Nov, 2009

GO_CONS_SST_PKI_2__20091101T235945_20091102T235944_0001 Times in UTC

Measurement Epochs

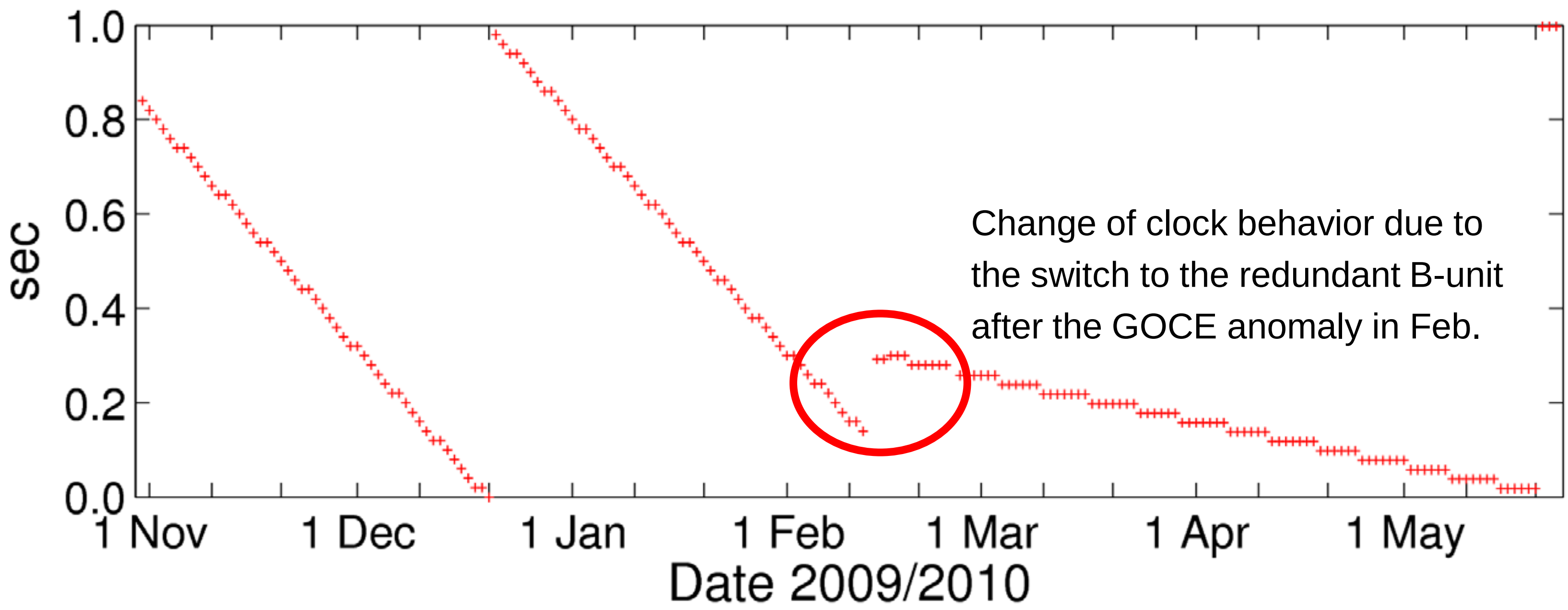

Fractional parts of measurement epochs:
The measurement sampling is 1 Hz, but the internal clock is not steered to integer seconds (fractional parts are shown in the figure for the midnight epochs).

Dynamic Orbit Representation (1)

Satellite position $\boldsymbol{r}_{leo}(t_{leo})$ (in inertial frame) is given by:

$$\boldsymbol{r}_{leo}(t_{leo}) = \boldsymbol{r}_{leo,0}(t_{leo}; a, e, i, \Omega, \omega, u_0; Q_1, ..., Q_d) + \delta\boldsymbol{r}_{leo,ant}(t_{leo})$$

$\boldsymbol{r}_{leo,0}$	LEO center of mass position
$\delta\boldsymbol{r}_{leo,ant}$	LEO antenna phase center offset
$a, e, i, \Omega, \omega, u_0$	LEO initial osculating orbital elements
$Q_1, ..., Q_d$	LEO dynamical parameters

Satellite trajectory $\boldsymbol{r}_{leo,0}$ is a particular solution of an **equation of motion**

- One set of **initial conditions** (orbital elements) is estimated per arc
  Dynamical parameters of the force model on request

Dynamic Orbit Representation (2)

Equation of motion (in inertial frame) is given by:

$$\ddot{\boldsymbol{r}} = -GM\frac{\boldsymbol{r}}{r^3} + \boldsymbol{f}_1(t, \boldsymbol{r}, \dot{\boldsymbol{r}}, Q_1, ..., Q_d)$$

with initial conditions

$$\boldsymbol{r}(t_0) = \boldsymbol{r}(a, e, i, \Omega, \omega, u_0; t_0)$$
$$\dot{\boldsymbol{r}}(t_0) = \dot{\boldsymbol{r}}(a, e, i, \Omega, \omega, u_0; t_0)$$

The **acceleration** $\boldsymbol{f}_1$ consists of **gravitational** and **non-gravitational** perturbations taken into account to model the satellite trajectory. Unknown parameters $Q_1, ..., Q_d$ of force models may appear in the equation of motion together with deterministic (known) accelerations given by analytical models.

Osculating Orbital Elements (1)

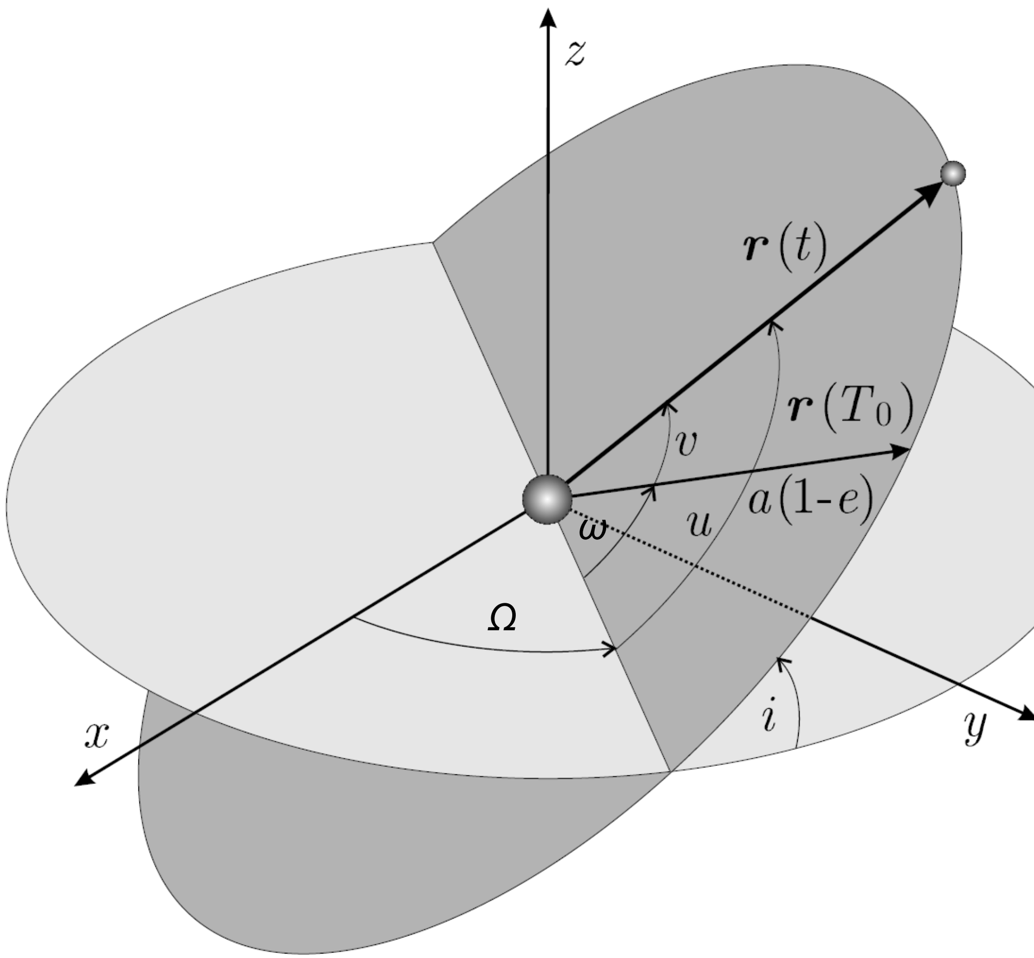

Osculating Orbital Elements of GOCE (2)

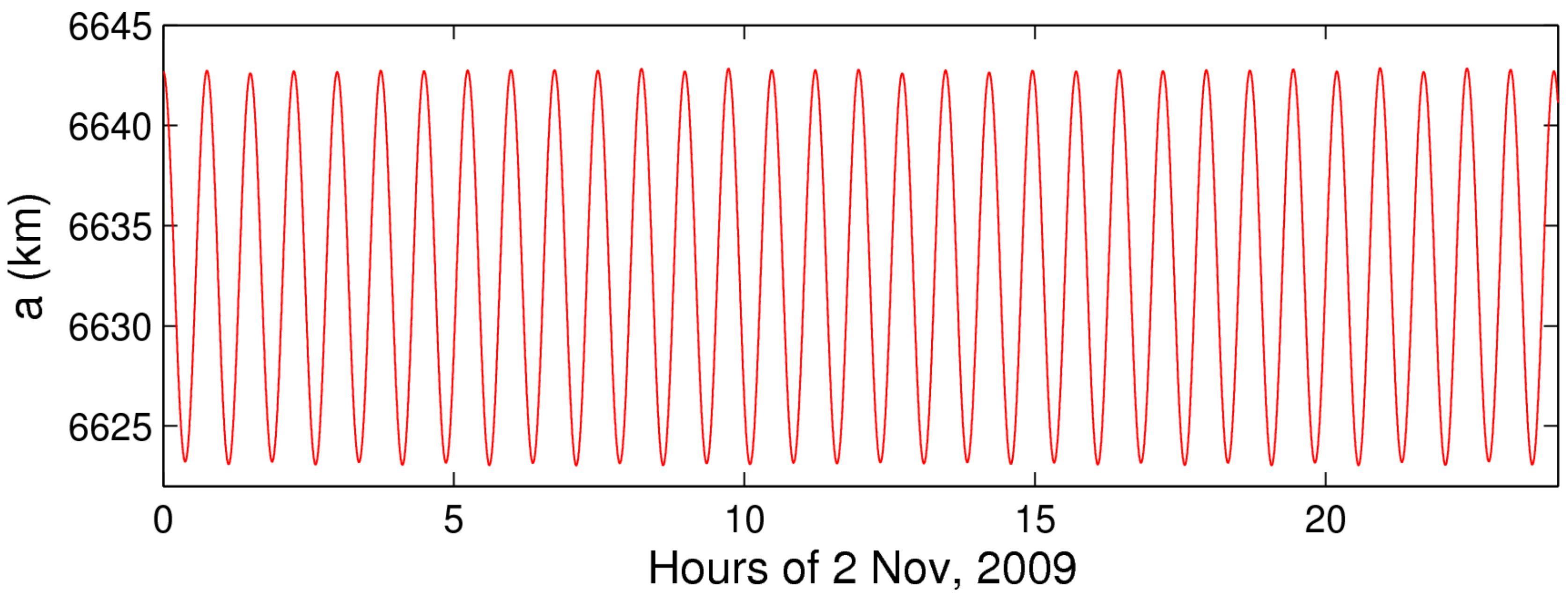

Semi-major axis:

Twice-per-revolution variations of about ±10 km around the mean semi-major axis of 6632.9km, which corresponds to the 254.9 km mean altitude used by ESA

Osculating Orbital Elements of GOCE (3)

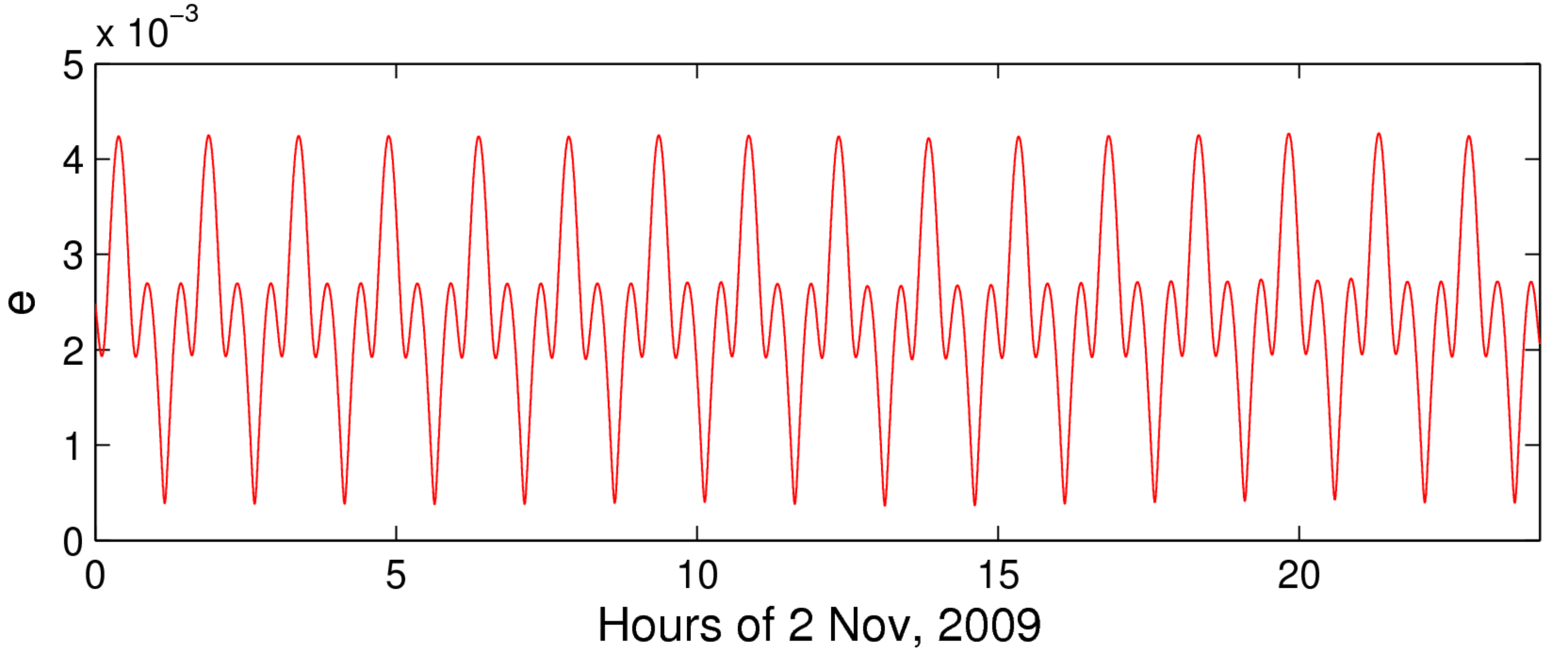

Numerical eccentricity:

Small, short-periodic variations around the mean value of about 0.0025, i.e., the orbit is close to circular

Osculating Orbital Elements of GOCE (4)

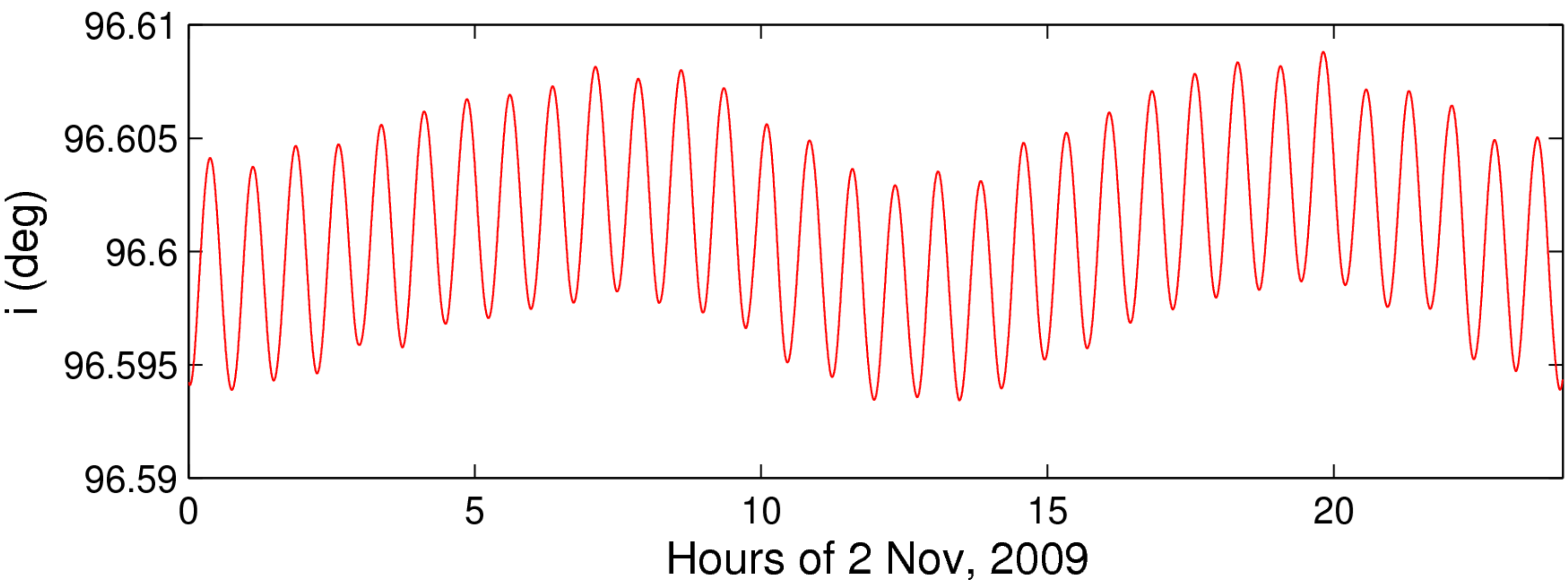

Inclination:

Twice-per-revolution and longer variations around the mean inclination of about 96.6° (sun-synchronous orbit)

Osculating Orbital Elements of GOCE (5)

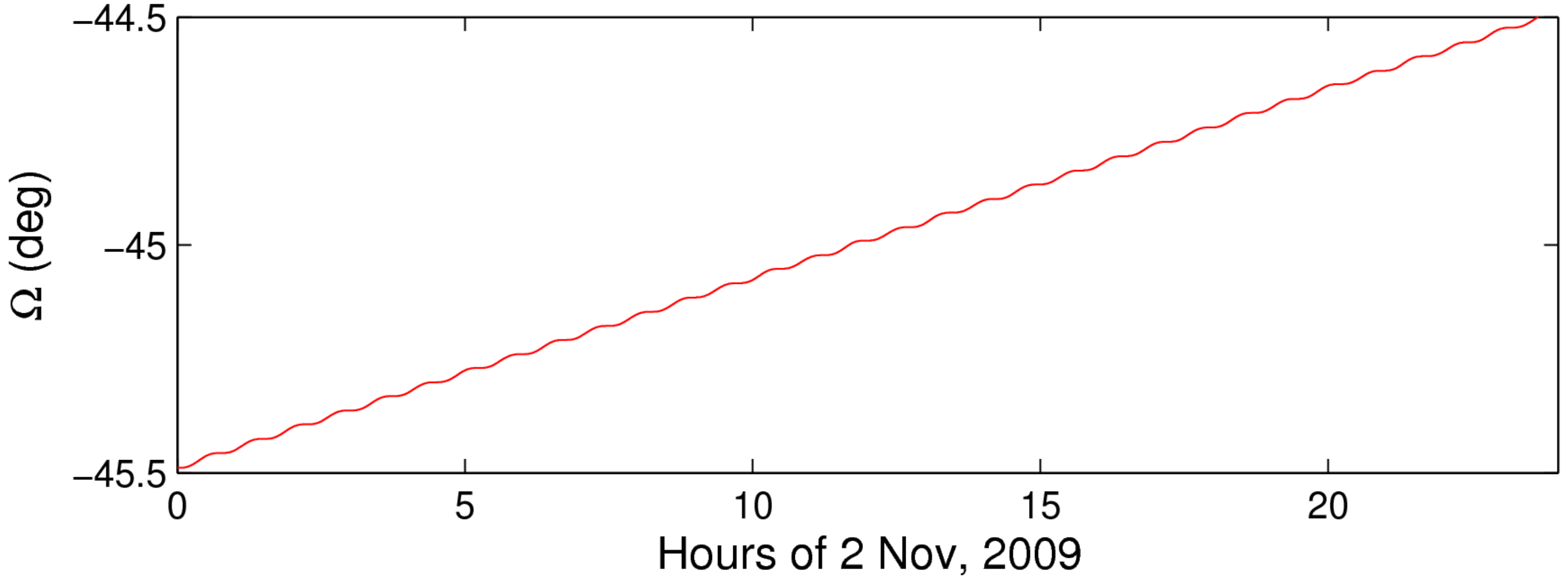

Right ascension of ascending node:

Twice-per-revolution variations and linear drift of about +1°/day (360°/365days) due to the sun-synchronous orbit

Dynamic Orbit Representation (3)

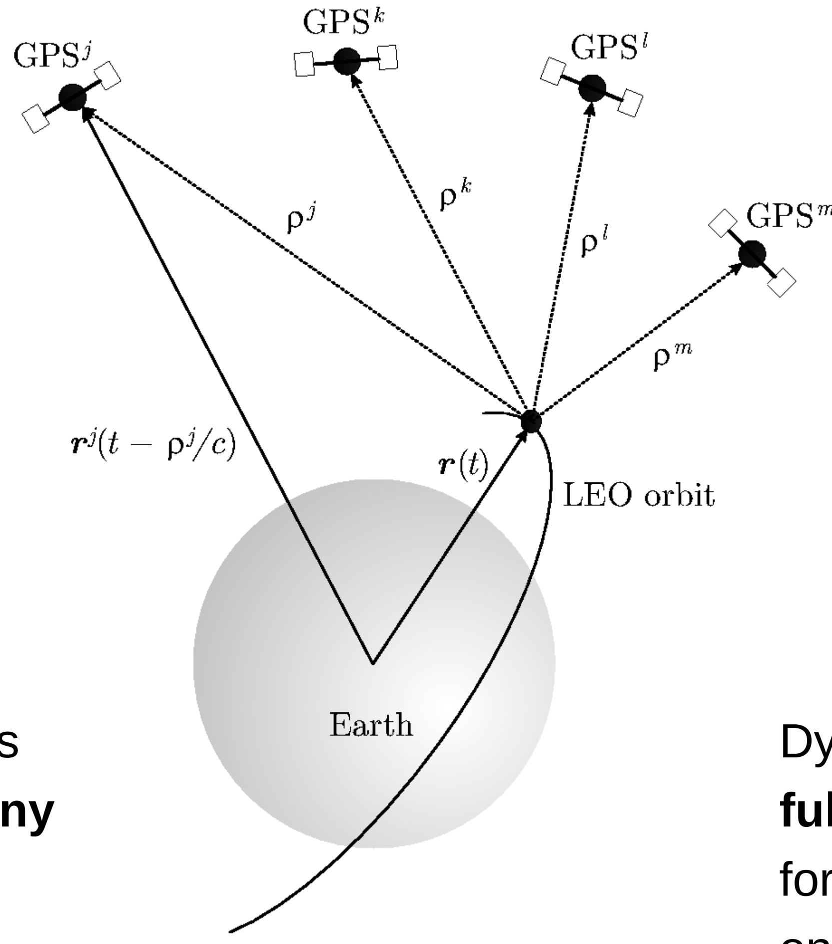

Dynamic orbit positions may be computed at **any epoch** within the arc

Dynamic positions are **fully dependent** on the force models used, e.g., on the gravity field model

Reduced-Dynamic Orbit Representation (1)

Equation of motion (in inertial frame) is given by:

$$\ddot{\boldsymbol{r}} = -GM\frac{\boldsymbol{r}}{r^3} + \boldsymbol{f}_1(t, \boldsymbol{r}, \dot{\boldsymbol{r}}, Q_1, ..., Q_d, P_1, ..., P_s)$$

$P_1, ..., P_s$ Pseudo-stochastic parameters

Pseudo-stochastic parameters are:

- additional empirical parameters characterized by a priori known **statistical properties**, e.g., by expectation values and a priori variances
- useful to **compensate** for deficiencies in dynamic models, e.g., deficiencies in models describing non-gravitational accelerations
- often set up as **piecewise constant accelerations** to ensure that satellite trajectories are continuous and differentiable at any epoch

Reduced-Dynamic Orbit Representation (2)

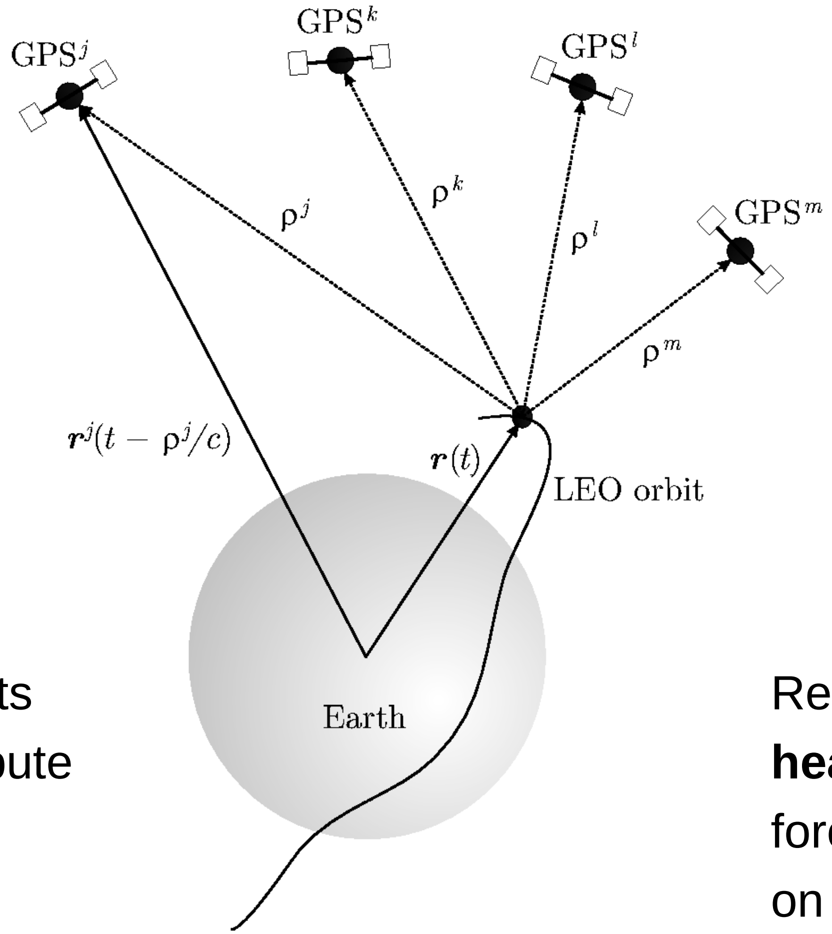

Reduced-dynamic orbits are well suited to compute LEO orbits of **highest quality**
(Jäggi et al., 2006; Jäggi, 2007)

Reduced-dynamic orbits **heavily depend** on the force models used, e.g., on the gravity field model
(Jäggi et al., 2008)

Partial Derivatives

Orbit improvement ($\boldsymbol{r}_0(t)$: numerically integrated **a priori orbit**):

$$\boldsymbol{r}(t) = \boldsymbol{r}_0(t) + \sum_{i=1}^{n} \frac{\partial \boldsymbol{r}_0}{\partial P_i}(t) \cdot (P_i - P_{0,i})$$

yields corrections to a priori parameter values $P_{0,i}$ by **least-squares**

Previously, for each parameter P_i the corresponding **variational equation**

$$\ddot{\boldsymbol{z}}_{P_i} = \boldsymbol{A}_0 \cdot \boldsymbol{z}_{P_i} + \boldsymbol{A}_1 \cdot \dot{\boldsymbol{z}}_{P_i} + \frac{\partial \boldsymbol{f}_1}{\partial P_i}$$

has to be solved to obtain the partials $\boldsymbol{z}_{P_i}(t) \doteq \frac{\partial \boldsymbol{r}_0}{\partial P_i}(t)$, e.g., by:

- Numerical integration for initial osculating elements
- Numerical quadrature for dynamic parameters
- Linear combinations for pseudo-stochastic parameters (Jäggi, 2007)

Reduced-dynamic Orbit Representation (3)

Position epochs
(in GPS time)

Positions (km) &
Velocities (dm/s)
(Earth-fixed)

```
*  2009 11  2  0  0  0.00000000
PL15   -391.718353   6623.836682     79.317661 999999.999999
VL15  13710.157683   1908.731015 -77015.601314 999999.999999
*  2009 11  2  0  0 10.00000000
PL15   -377.980705   6625.284690      2.298385 999999.999999
VL15  13764.602016    987.250587 -77021.193676 999999.999999
*  2009 11  2  0  0 20.00000000
PL15   -364.190222   6625.811136    -74.721213 999999.999999
VL15  13815.825127     65.631014 -77016.232293 999999.999999
*  2009 11  2  0  0 30.00000000
PL15   -350.350131   6625.415949   -151.730567 999999.999999
VL15  13863.820409   -855.995477 -77000.719734 999999.999999
*  2009 11  2  0  0 40.00000000
PL15   -336.463660   6624.099187   -228.719134 999999.999999
VL15  13908.581905  -1777.497047 -76974.660058 999999.999999
*  2009 11  2  0  0 50.00000000
PL15   -322.534047   6621.861041   -305.676371 999999.999999
VL15  13950.104280  -2698.741871 -76938.058807 999999.999999
*  2009 11  2  0  1  0.00000000
PL15   -308.564533   6618.701833   -382.591743 999999.999999
VL15  13988.382807  -3619.598277 -76890.923043 999999.999999
```

Clock corrections
are not provided

Excerpt of reduced-dynamic GOCE positions at begin of 2 Nov, 2009

GO_CONS_SST_PRD_2__20091101T235945_20091102T235944_0001

LEO Sensor Offsets (1)

Phase center offsets $\delta \boldsymbol{r}_{leo,ant}$:

- are needed in the inertial or Earth-fixed frame and have to be transformed from the satellite frame using **attitude data** from the star-trackers
- consist of a frequency-independent **instrument offset**, e.g., defined by the center of the instrument‘s mounting plane (CMP) in the satellite frame
- consist of frequency-dependent **phase center offsets** (PCOs), e.g., defined wrt the center of the instrument‘s mounting plane in the antenna frame (ARF)
- consist of frequency-dependent **phase center variations** (PCVs) varying with the direction of the incoming signal, e.g., defined wrt the PCOs in the antenna frame

LEO Sensor Offsets (2)

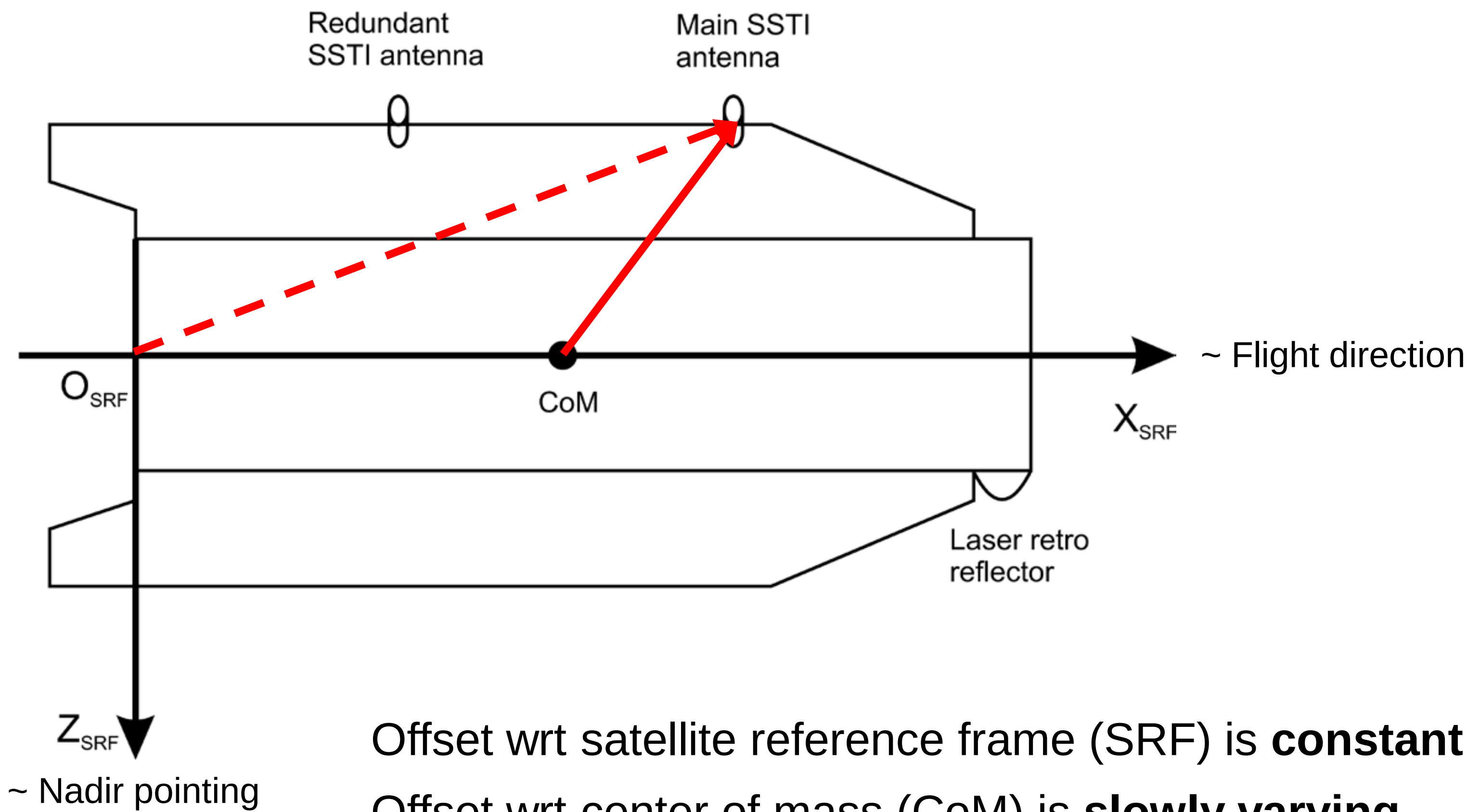

Offset wrt satellite reference frame (SRF) is **constant**

Offset wrt center of mass (CoM) is **slowly varying**

GOCE Sensor Offsets

Table 1: CoM coordinates in SRF system

CoM	X_{SRF}[m]	Y_{SRF}[m]	Z_{SRF}[m]
Begin of Life (BoL)	2.4990	0.0036	0.0011
End of Life (EoL)	2.5290	0.0038	0.0012

Table 2: SSTI antenna CMP coordinates in SRF system

CMP coordinates	X_{SRF} [m]	Y_{SRF}[m]	Z_{SRF}[m]
Main	3.1930	0.0000	-1.0922
Redundant	1.3450	0.0000	-1.0903

Table 3: SSTI antenna CMP coordinates wrt to CoM (BoL)

CMP coordinates	X_{CoM} [m]	Y_{CoM}[m]	Z_{CoM}[m]
Main	0.6940	-0.0036	-1.0933
Redundant	-1.1540	-0.0036	-1.0914

Table 4: SSTI antenna phase center offsets in ARF system

Phase center offsets	X_{ARF}[mm]	Y_{ARF}[mm]	Z_{ARF}[mm]
Main: L1	-0.18	3.51	-81.11
Main: L2	-1.22	-1.00	-84.18
Redundant: L1	-0.96	3.14	-81.33
Redundant: L2	-1.48	-1.20	-84.18

Derived from Bigazzi and Frommknecht (2010)

GOCE GPS Antenna

L1, L2, Lc phase center offsets

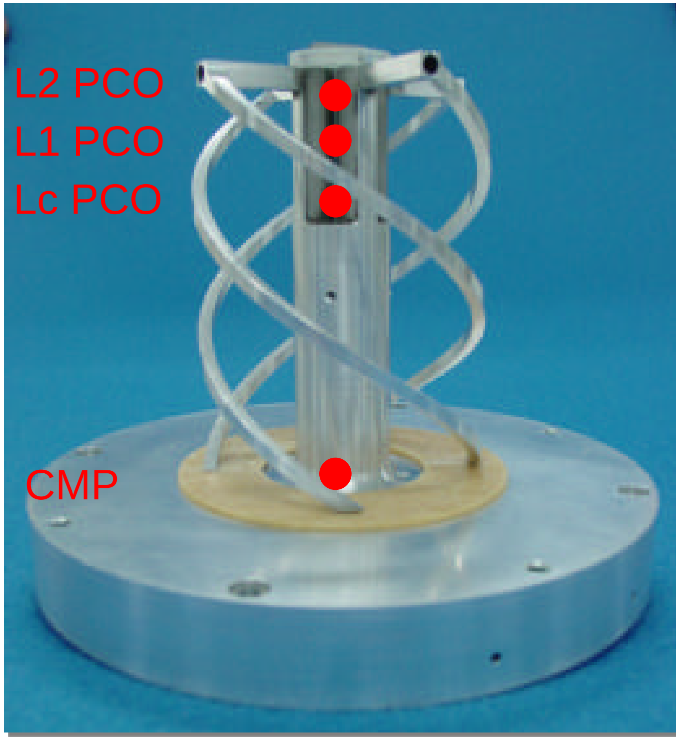

Measured from ground calibration in anechoic chamber

Lc phase center variations

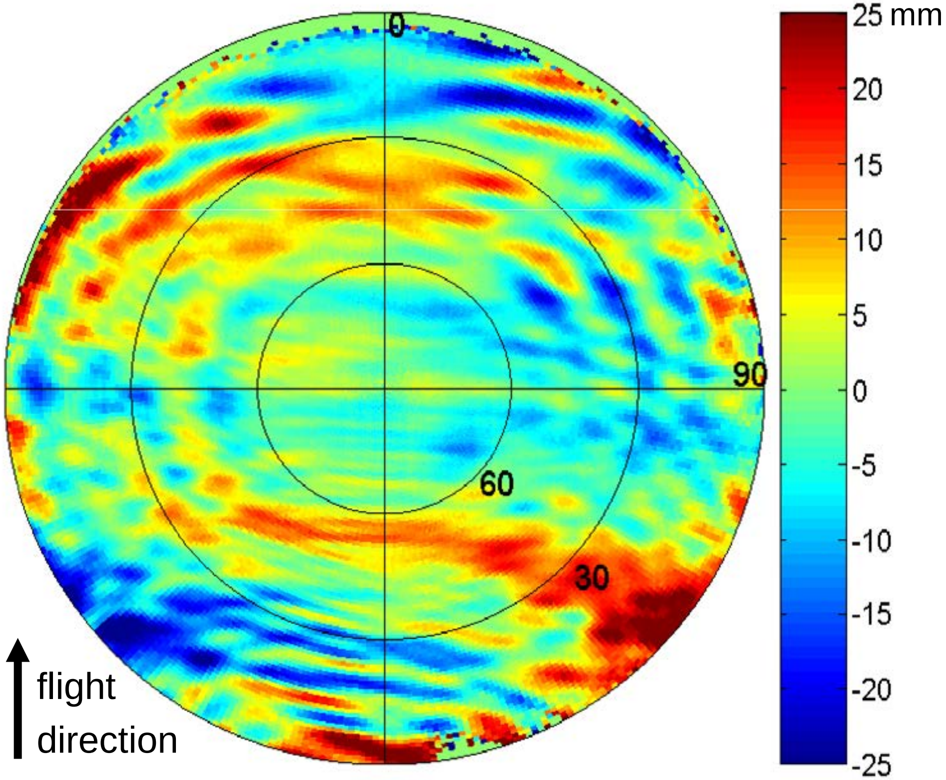

Empirically derived during orbit determination according to Jäggi et al. (2009)

Other spaceborne GPS antennas

Lc phase center variations

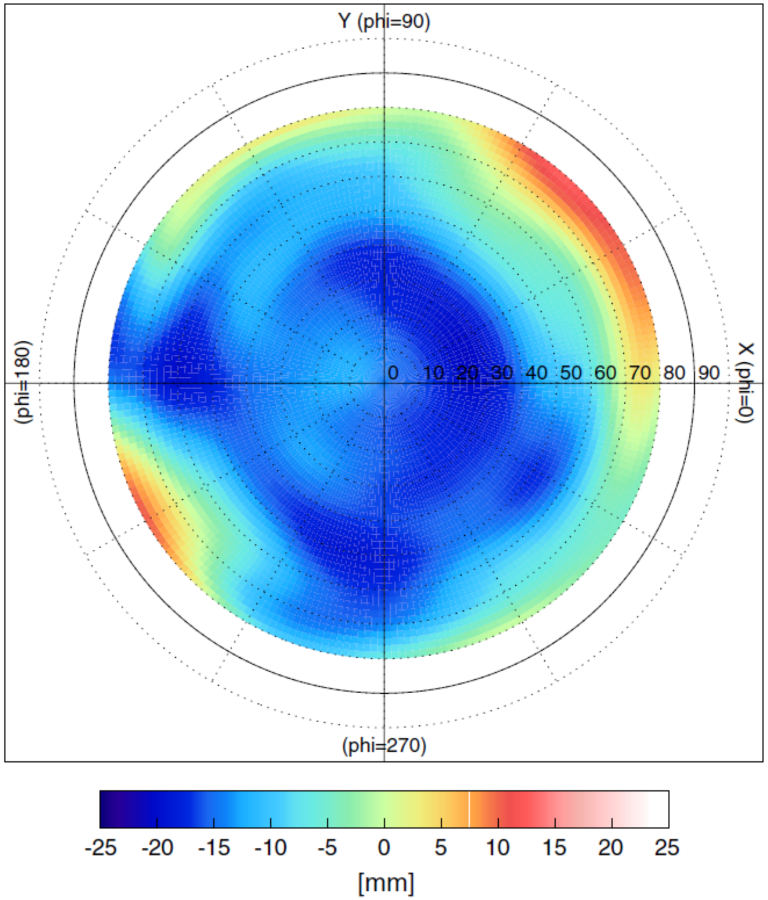

Measured from ground calibration in anechoic chamber

Lc phase center corrections

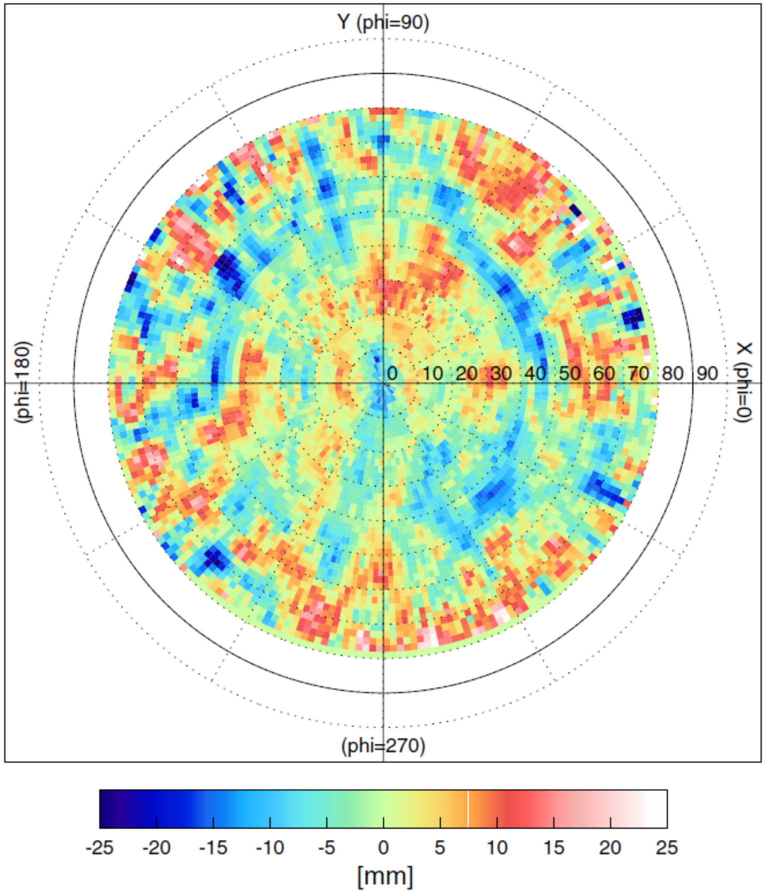

Empirically derived during orbit determination according to Montenbruck et al. (2008)

GOCE High-level Processing Facility: Orbit Groups

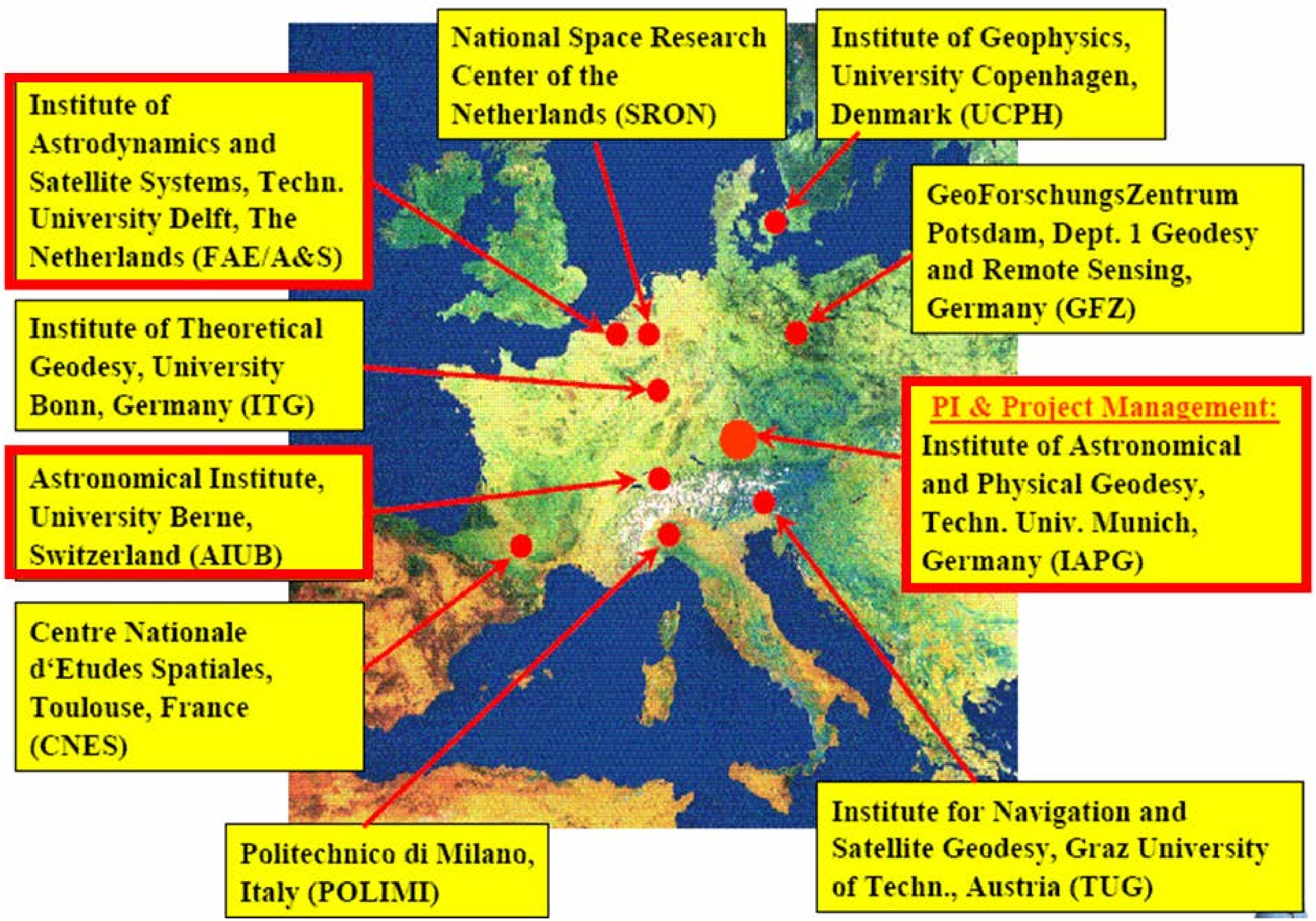

Responsibilities:

DEOS => **RSO**
(Rapid Science Orbit)

AIUB => **PSO**
(Precise Science Orbit)

IAPG => Validation

GOCE High-level Processing Facility: Orbit Products

	Orbit solution	Software	GPS Observ.	GPS products	Sampling	Data batches	Latency
RSO	reduced-dynamic	GEODYN	triple-diff	IGS	10 sec	30 h	1 day
	kinematic	GHOST	zero-diff	rapid	1 sec	24 h	1 day
PSO	reduced-dynamic	BERNESE	zero-diff	CODE	10 sec	30 h	7-10 days
	kinematic	BERNESE	zero-diff	final	1 sec	30 h	7-10 days

Accuracy requirement: 50 cm

Accuracy requirement: 2 cm

(Visser et al., 2009) (Bock et al., 2011)

Visualization of LEO Orbit Products

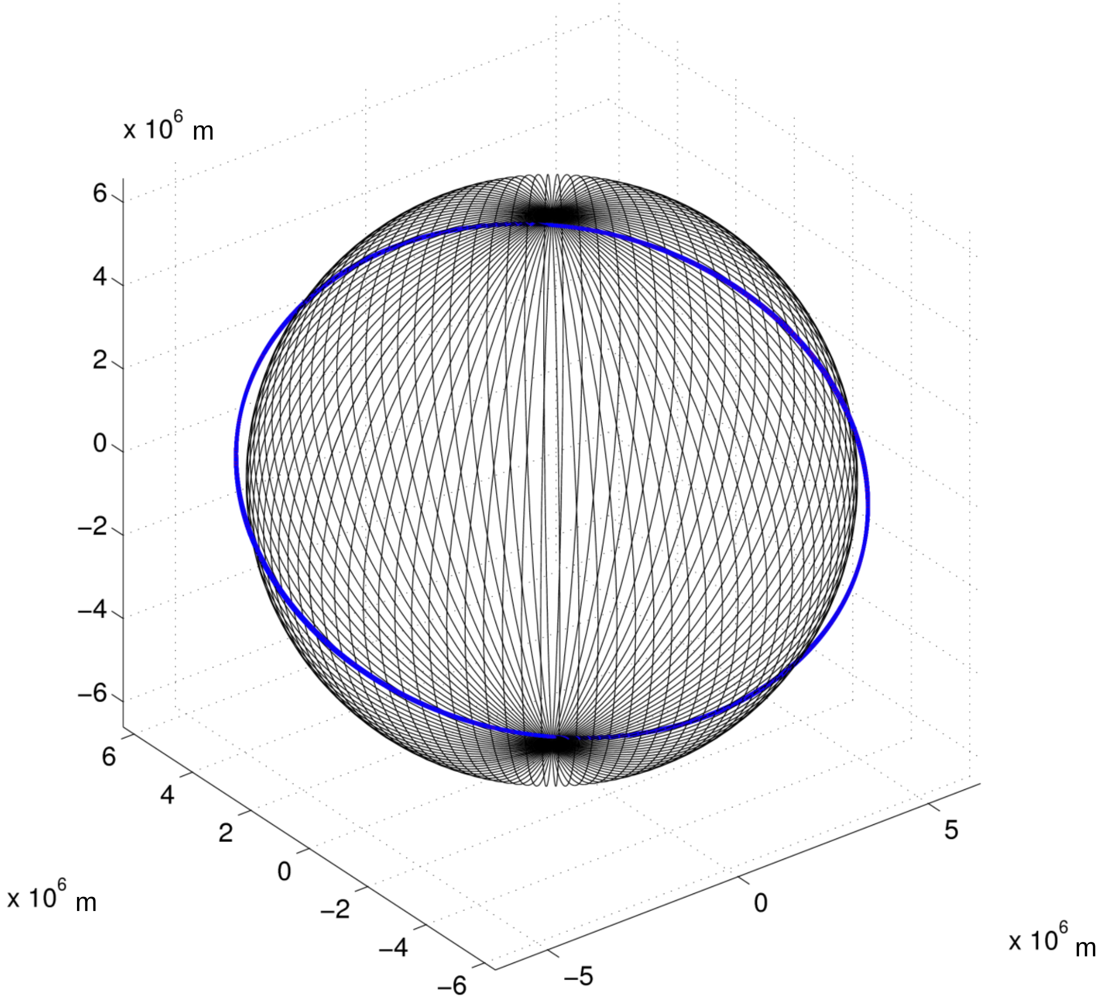

It is more instructive to look at differences between orbits in well suited coordinate systems …

Co-Rotating Orbital Frames

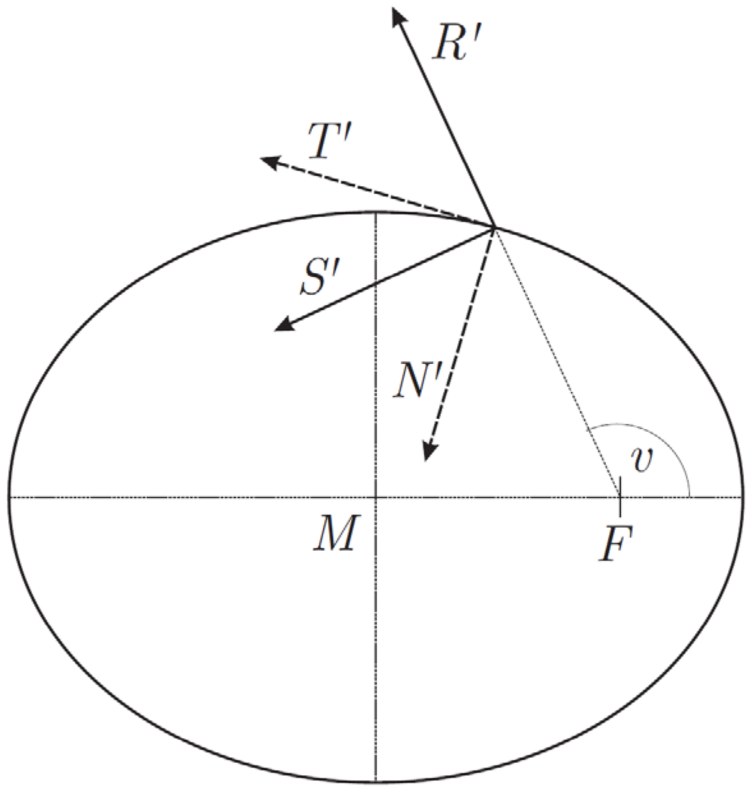

R, S, C unit vectors are pointing:
- into the radial direction
- normal to **R** in the orbital plane
- normal to the orbital plane (cross-track)

T, N, C unit vectors are pointing:
- into the tangential (along-track) direction
- normal to **T** in the orbital plane
- normal to the orbital plane (cross-track)

Small eccentricities: **S**~**T** (velocity direction)

GOCE Orbit Differences KIN-RD

Differences at epochs of kin. positions

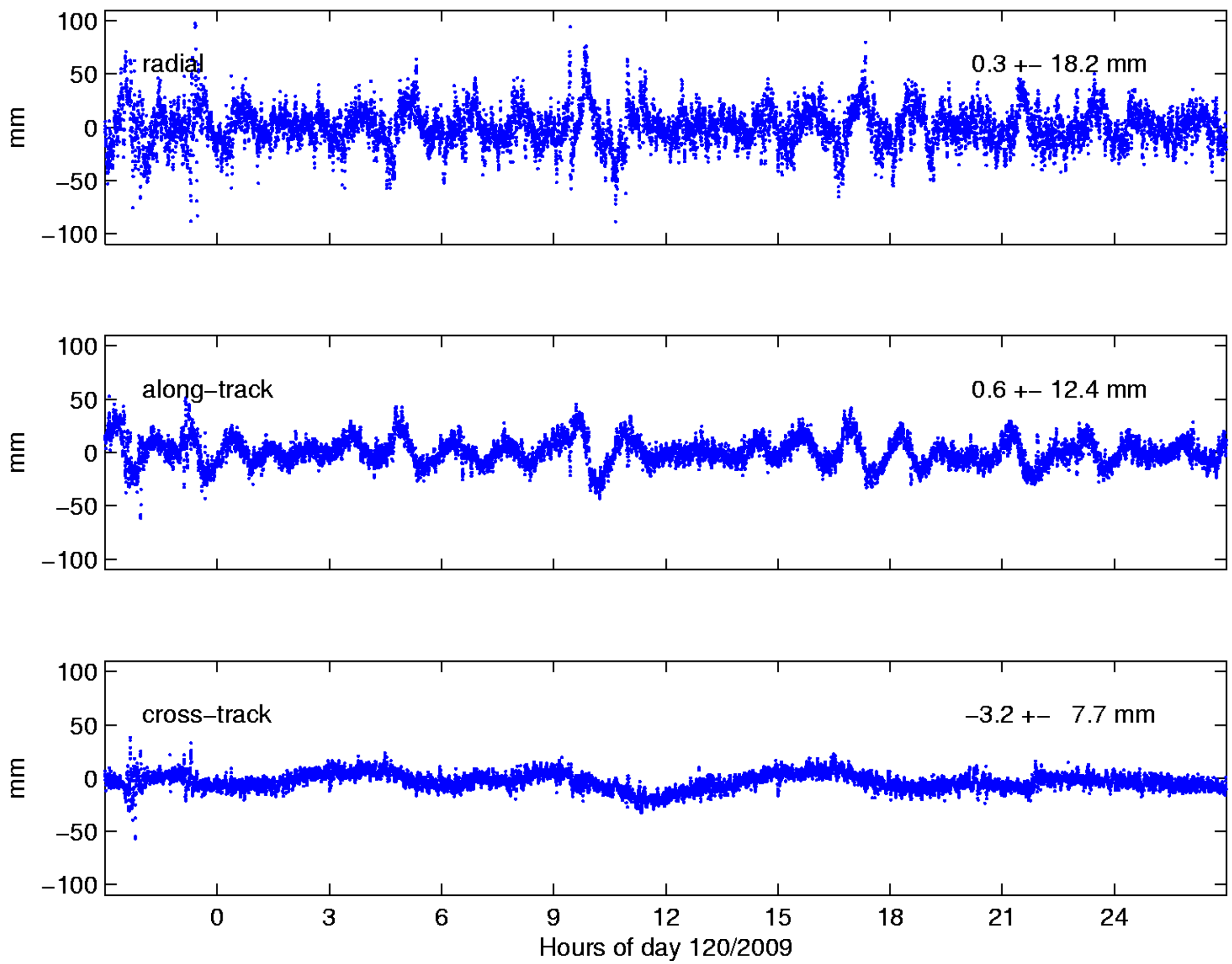

Orbit Differences KIN-RD, Time-Differenced

Largest scatter of kin. positions

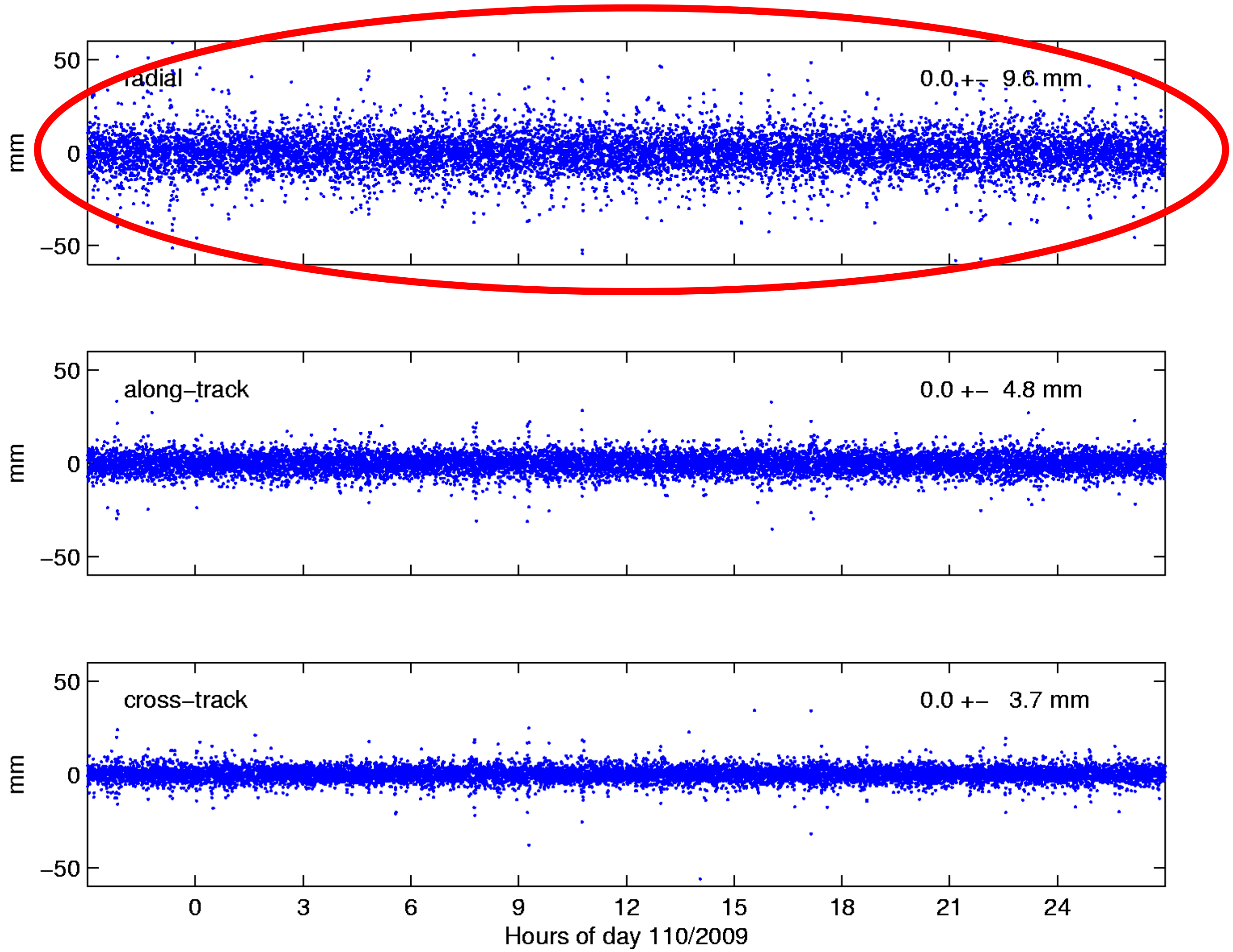

GOCE Pseudo-Stochastic Accelerations

Largest signal due to air drag

First drag-free flight on 7 May

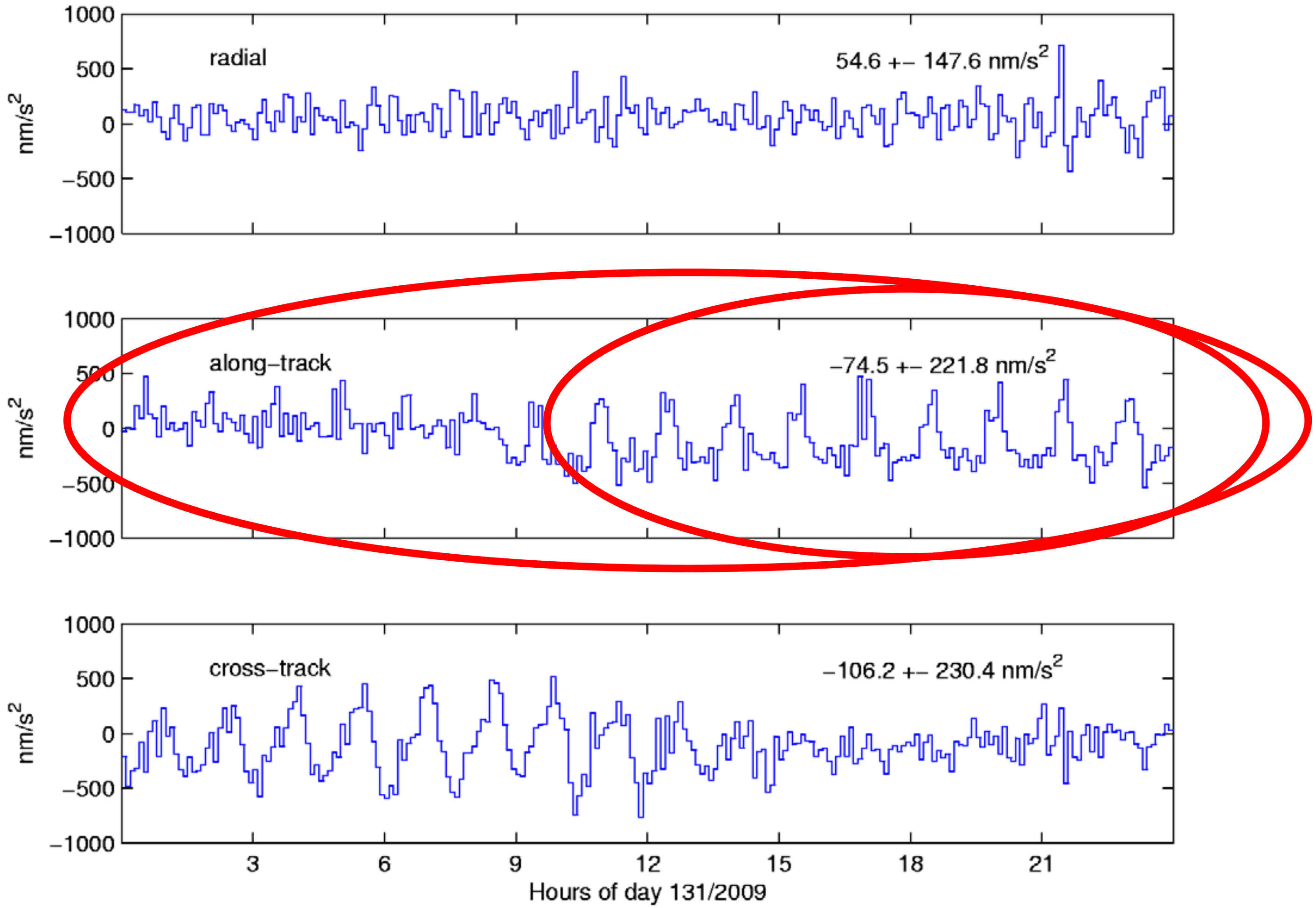

GOCE Orbital Altitude at Mission Begin

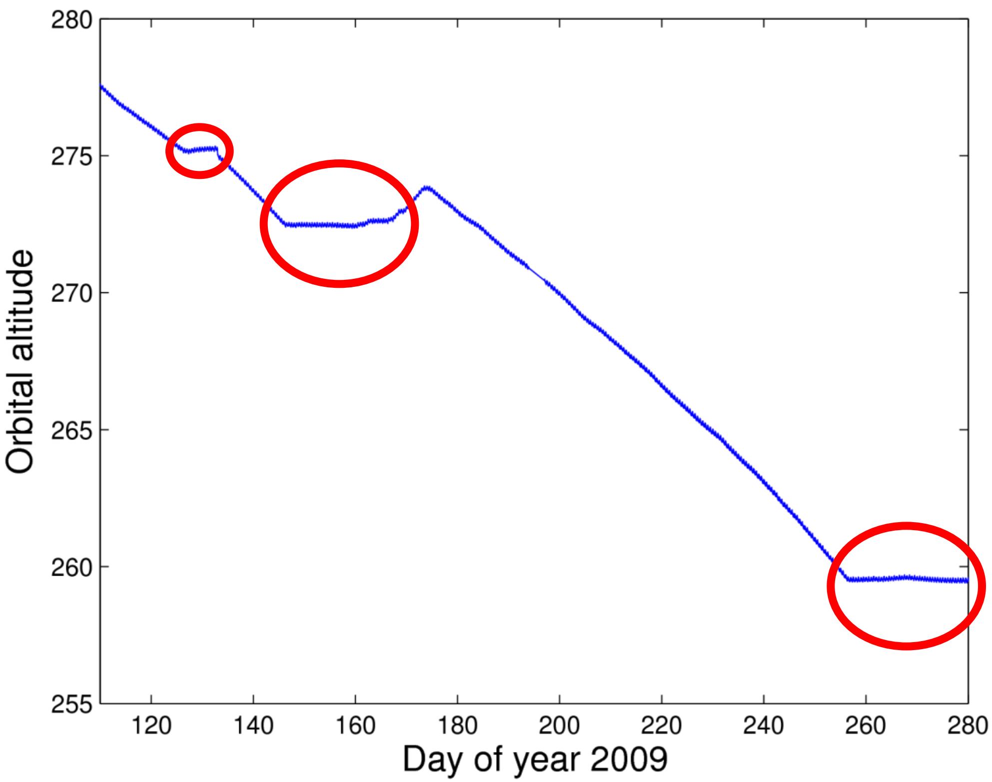

GOCE „History“:

17 March:
Launch into a sun-synchronous (i ~ 97°), dusk-dawn orbit at an altitude of 287.9 km

7 May:
First drag-free flight

26 May:
Second drag-free flight with various activities on gradiometer calibration

13/14 September:
Arrival at final orbital altitude of 259.6 km (254.9 km), start of drag-free flight for first Measurement and Operational Phase (MOP-1)

Improving GOCE Orbit Determination (1)

PCV modeling is one of the limiting factors for most precise LEO orbit determination. Unmodeled PCVs are systematic errors, which

- **directly** propagate into kinematic orbit determination and severly degrade the position estimates

- propagate into reduced-dynamic orbit determination to a smaller, **but still large extent**

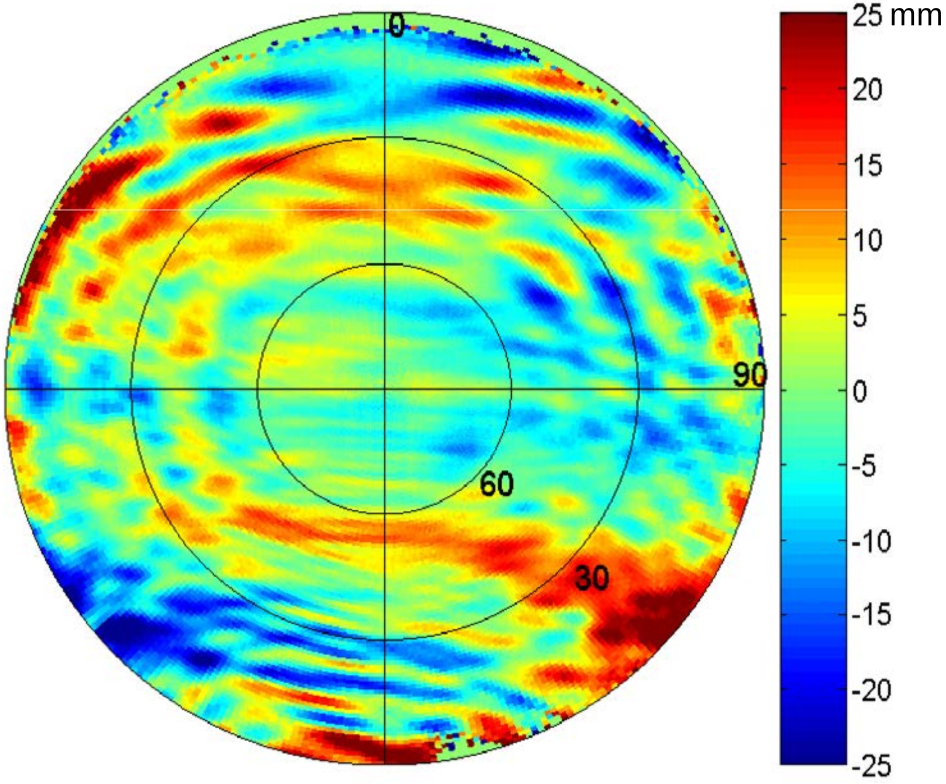

Improving GOCE Orbit Determination (2)

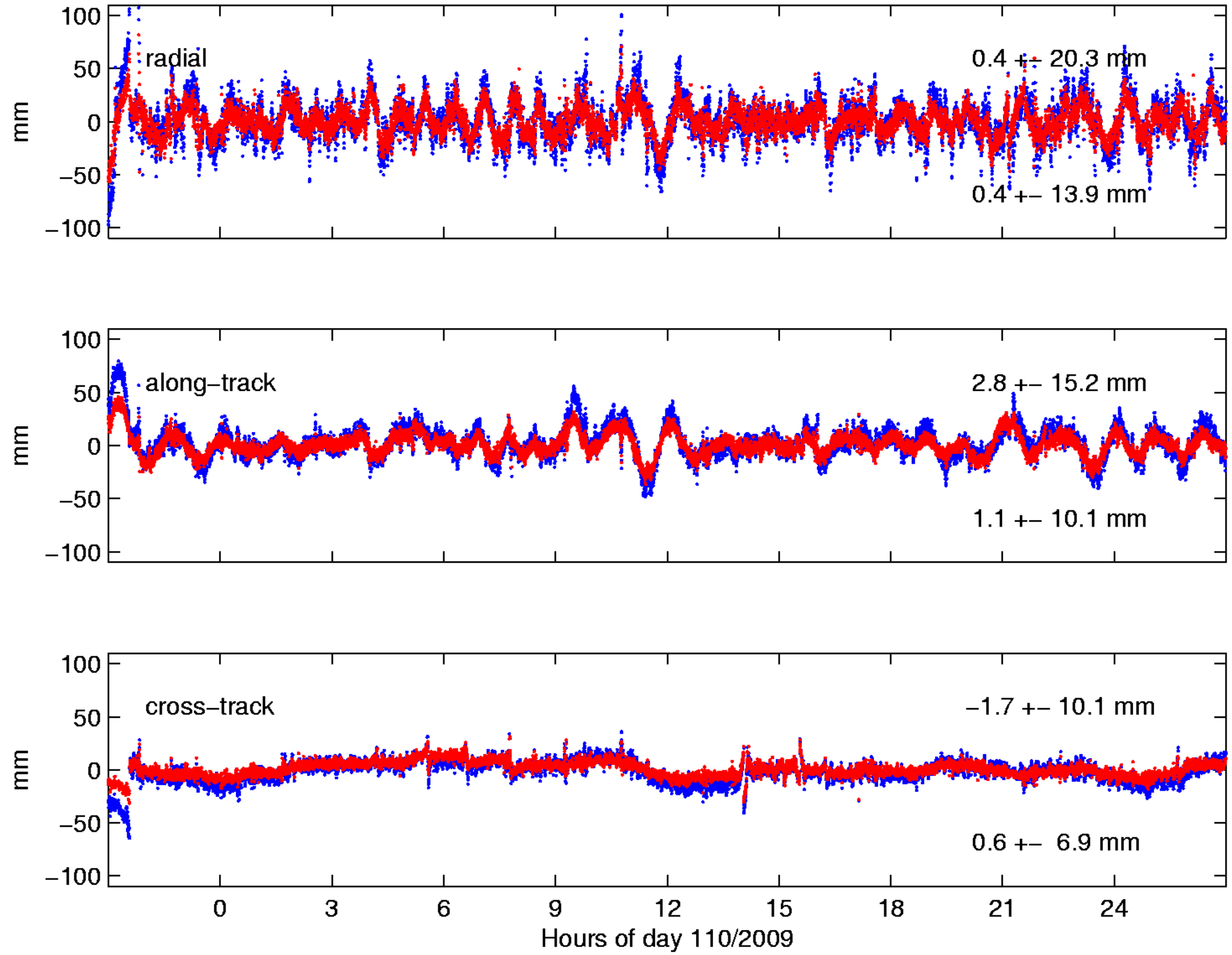

w/o PCV

with PCV

Improving GRACE Orbit Determination (1)

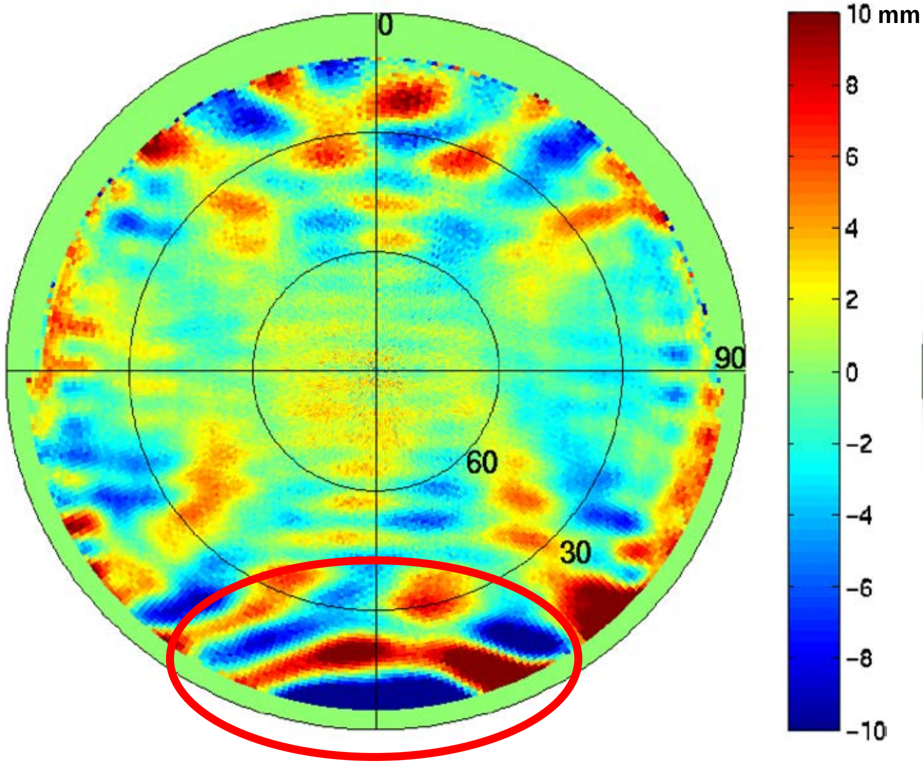

GRACE-A antenna

cross-talk of active occultation antenna

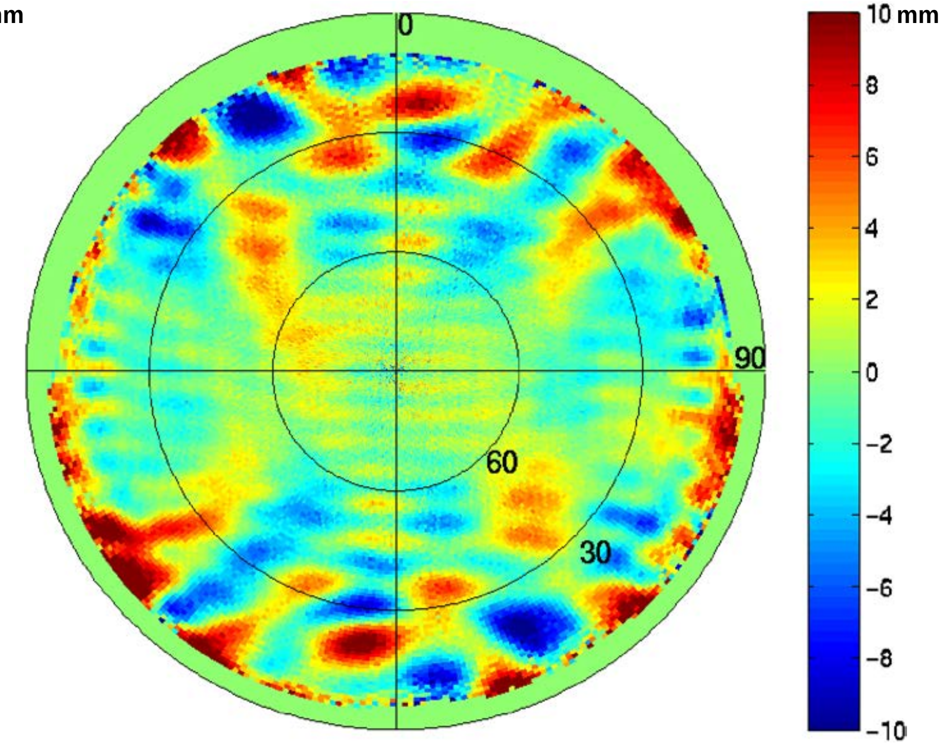

GRACE-B antenna

Improving GRACE Orbit Determination (2)

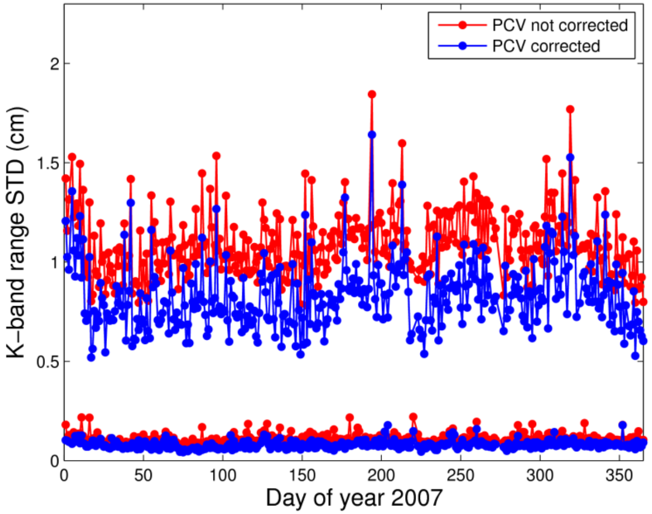

Orbit Determination

- independent validation with K-Band data (measurements with micrometer accuracy)
- Improvement of single-satellite solutions
- Improvement of baseline solutions

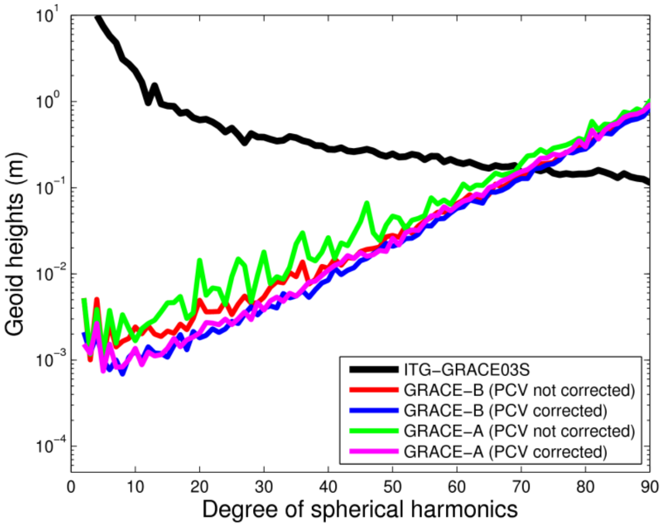

Gravity Field Determination

- independent validation wrt GRACE K-Band solutions
- Improvement of low degrees
- larger effect for GRACE-A (active RO-antenna)

Single-Frequency Orbit Determination

Reduced-Dynamic Orbit Determination

Mean 3D RMS [cm] of the orbit differences with respect to DF reference solution for days 273–279/2007 (=September 30–October 6, 2007) for different reduced-dynamic orbit solutions; for solutions A, B and C, improvement [%] with respect to solution "w/o".

LEO	Altitude	Solution						
	[km]	"w/o"	A		**B**		C	
GRACE A	470	134.3	63.7	52.6%	**19.6**	**85.4%**	20.5	84.7%
GRACE B	470	113.1	53.2	53.0%	**9.4**	**91.2%**	10.1	91.1%
MetOp-A	820	62.6	39.0	37.7%	**20.2**	**67.7%**	22.1	64.7%

Kinematic Orbit Determination

(Bock et al., 2009b)

Mean 3D RMS [cm] of the orbit differences with respect to DF reference solution for days 273–279/2007 (=September 30–October 6, 2007) for different kinematic orbit solutions; for solutions A, B and C, improvement [%] with respect to solution "w/o".

LEO	Altitude	Solution						
	[km]	"w/o"	A		**B**		C	
GRACE A	470	138.6	95.3	31.2%	**54.9**	**60.4%**	55.2	60.2%
GRACE B	470	119.0	87.2	26.7%	**32.8**	**72.4%**	33.5	71.8%
MetOp-A	820	85.6	**53.0**	**38.1%**	67.8	20.8%	68.1	20.4%

The so-called **GRAPHIC** (**GR**oup **A**nd **PH**ase **I**onospheric **C**orrection) linear combination **0.5·(L1 + C1)** was formed to compute solution B

Near Real-Time Orbit Determination

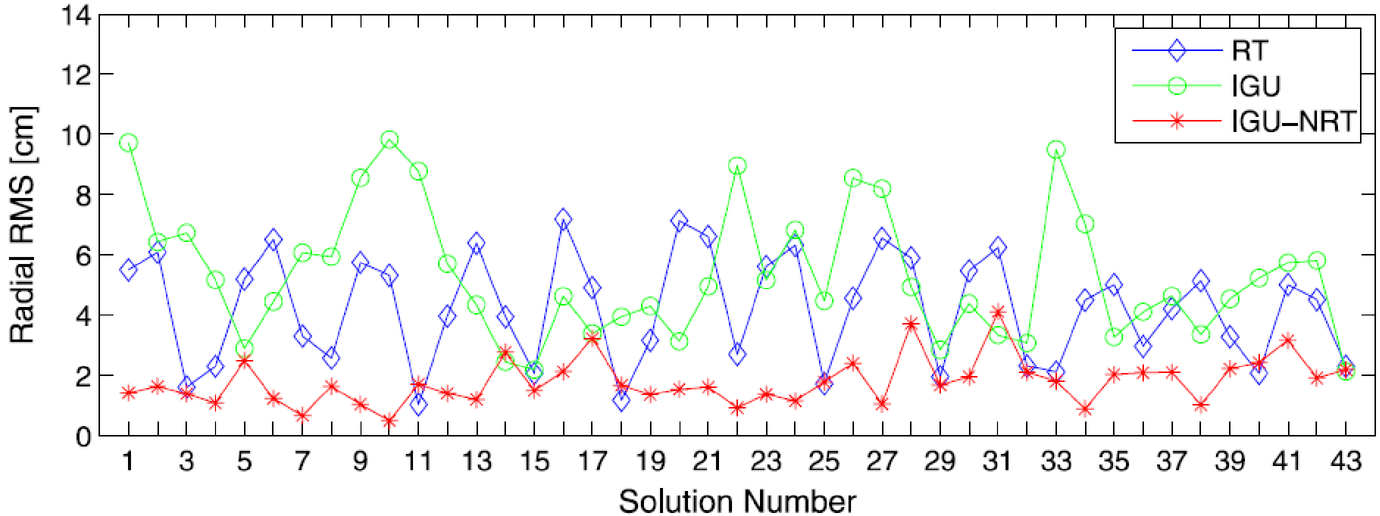

GRACE NRT Orbit Determination:

Based on NRT clock determination and IGS Ultra-Rapid (IGU) orbit products, 2cm radial RMS errors wrt post-processed orbits were achieved by Bock et al. (2009a)

MetOp-A NRT / RT Orbit Determination:

Velocity errors of better than 0.05 mm/s for NRT and 0.2 mm/s for real-time orbit determination were recently demonstrated by Montenbruck et al. (2012)

Orbit Validation by Satellite Laser Ranging (SLR)

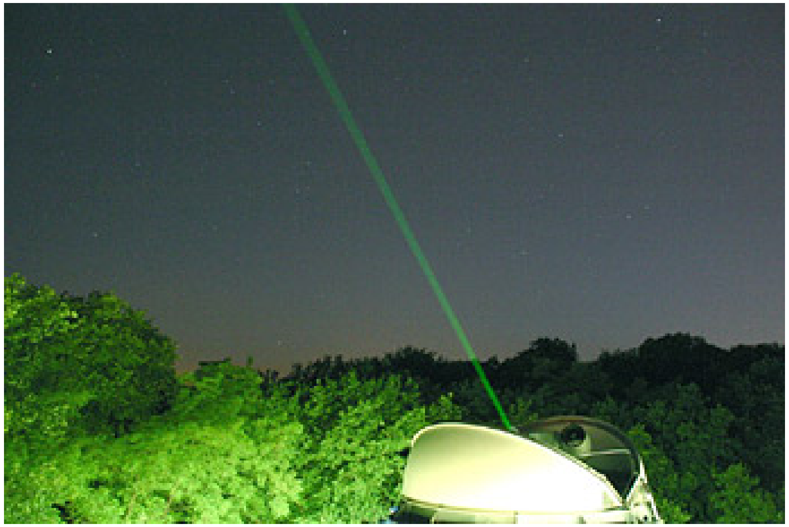

GFZ SLR station in Potsdam, Germany

AIUB SLR station in Zimmerwald, Switzerland

GOCE Orbit Accuracy from SLR Residuals (1)

LEO orbits may be shifted up to several cm‘s in the cross-track direction by unmodeled PCVs.

Thanks to the low orbital altitude of GOCE it could be confirmed for the first time with SLR data that the PCV-induced cross-track shifts are real (see measurements from the SLR stations in the east and west directions at low elevations).

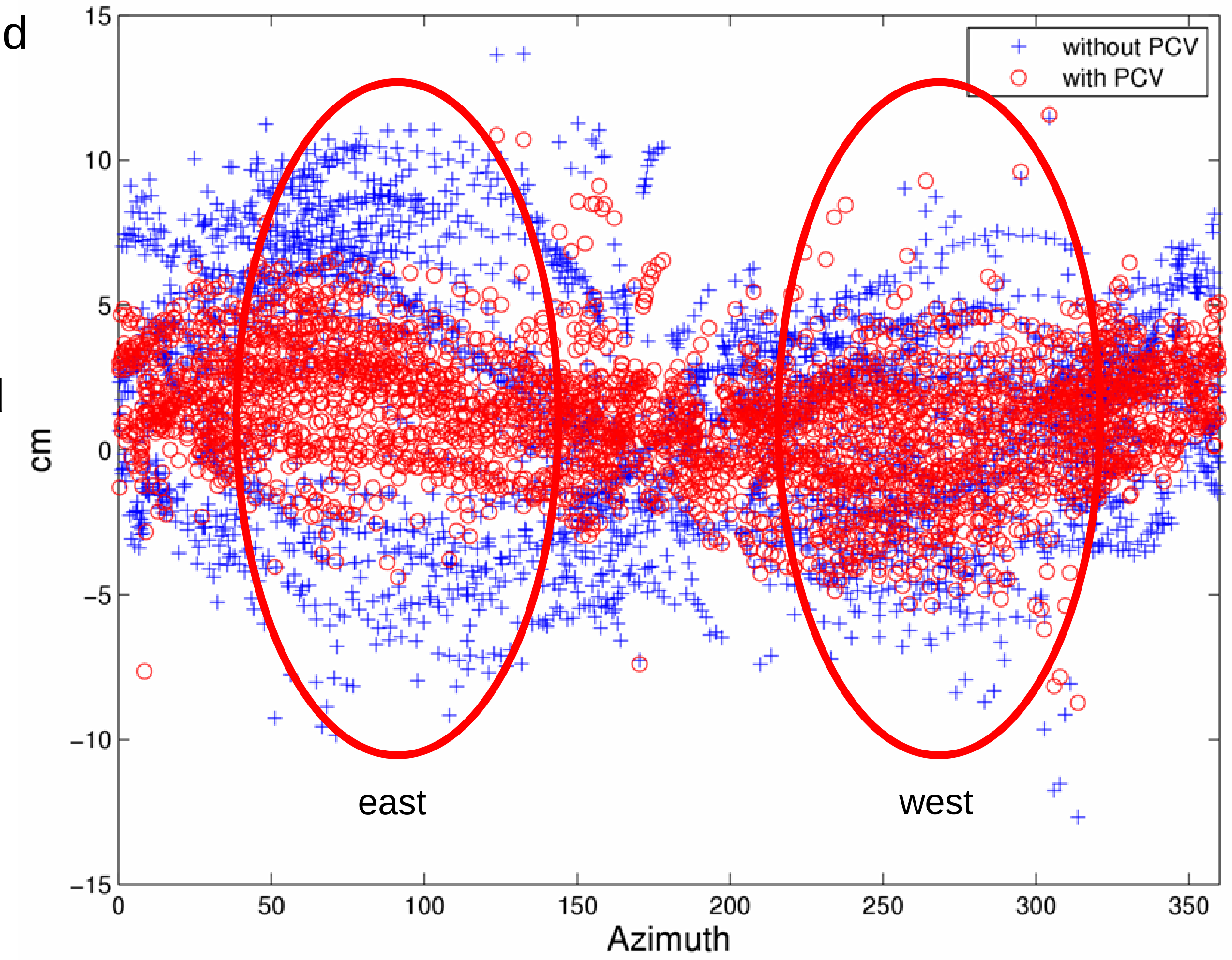

GOCE Orbit Accuracy from SLR Residuals (2)

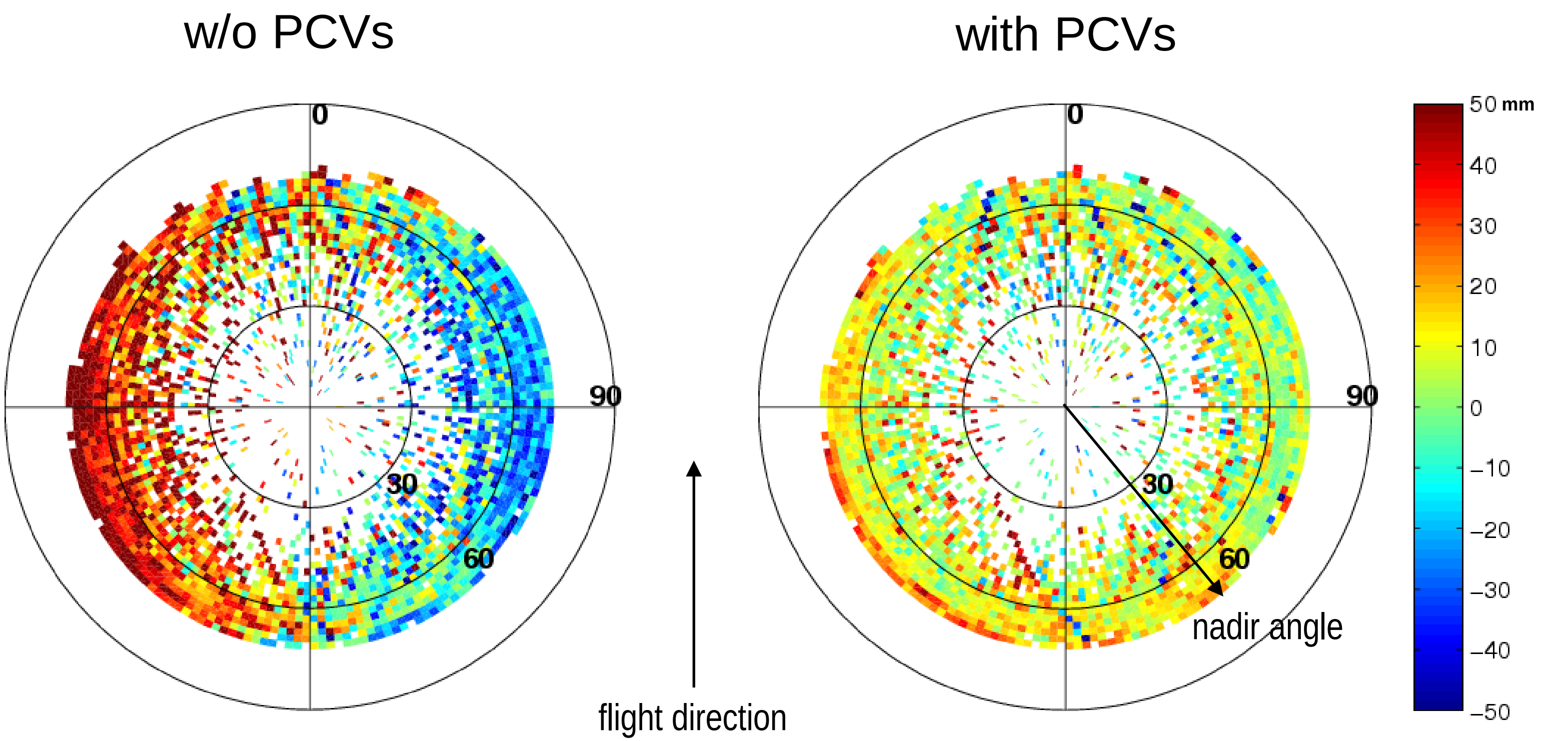

The PCV-induced cross-track shifts are best visualized when plotting the SLR residuals in a **satellite-fixed** coordinate system. This illustrates that SLR is not only able to detect radial biases.

GOCE Orbit Accuracy from SLR Residuals (3)

Reduced-dynamic orbit **Mean: 0.24 cm, RMS: 1.62 cm**

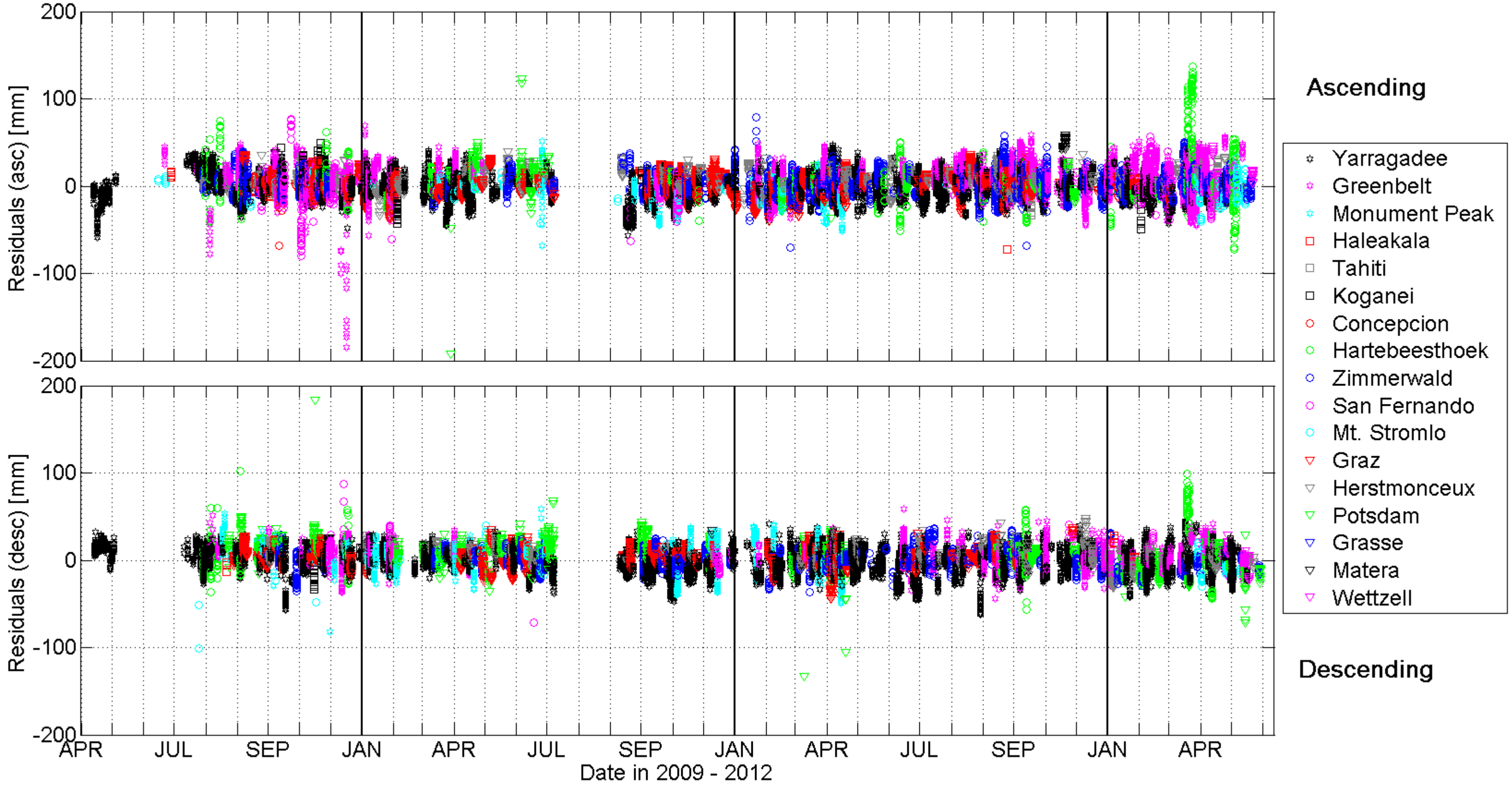

	2009:	2010:	2011:	2012:
RMS:	1.61 cm	1.44 cm	1.99 cm	2.05 cm
Mean:	0.46 cm	0.13 cm	0.25 cm	0.13 cm

GOCE Orbit Accuracy from SLR Residuals (4)

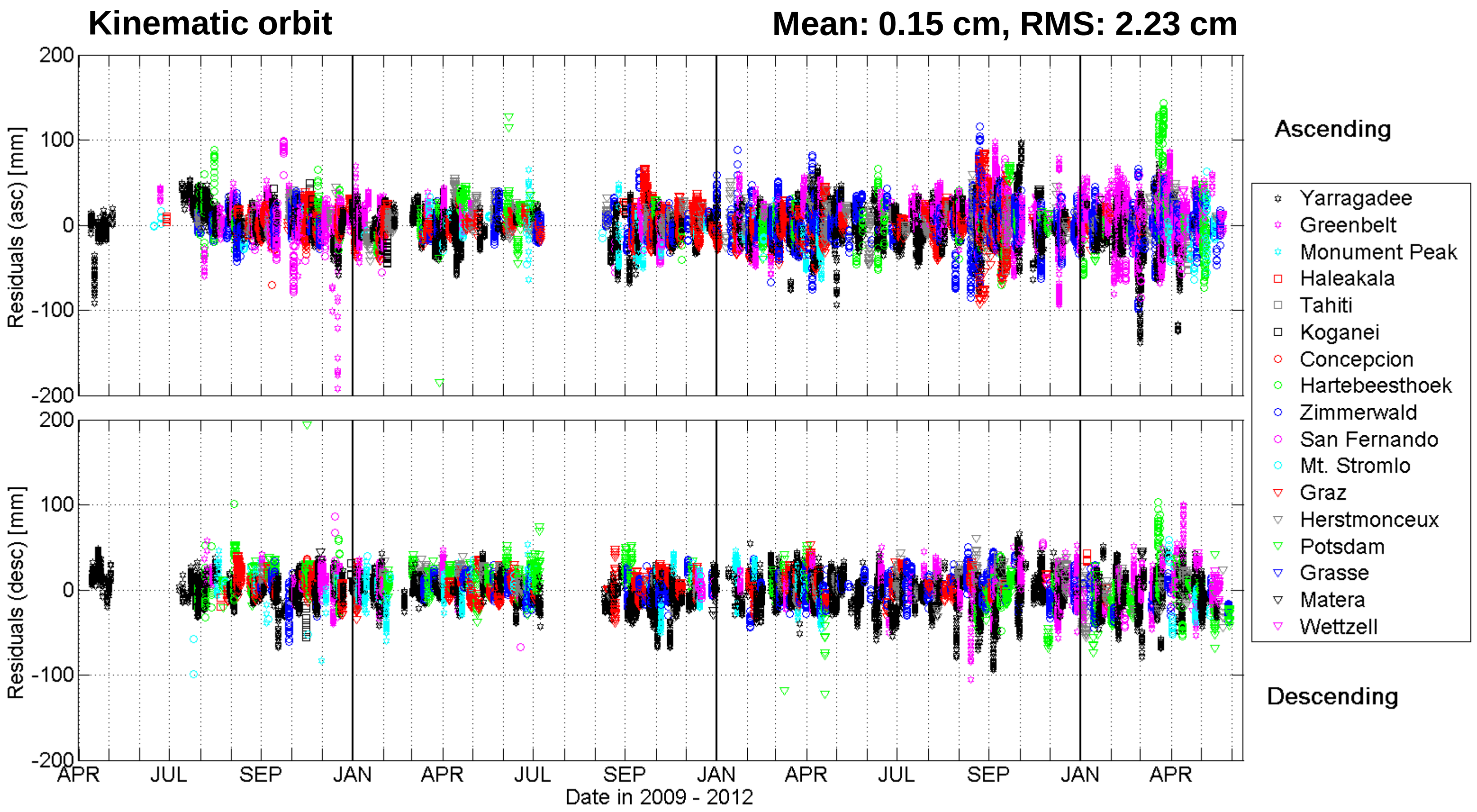

	2009:	2010:	2011:	2012:
RMS:	1.89 cm	1.76 cm	2.63 cm	3.00 cm
Mean:	0.49 cm	0.10 cm	0.15 cm	-0.24 cm

Orbit Differences KIN-RD on 2 Nov, 2009 (1)

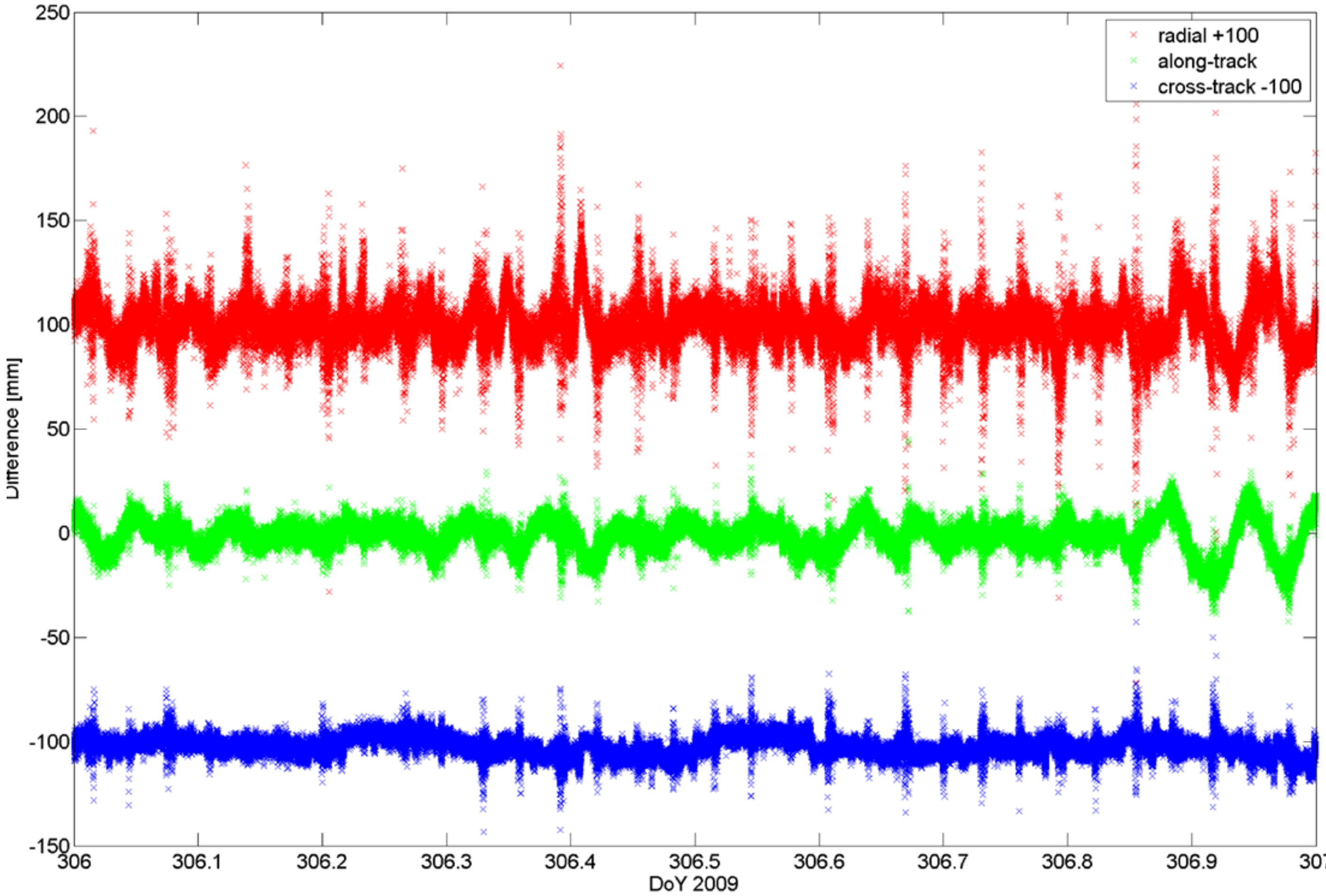

Orbit Differences KIN-RD on 2 Nov, 2009 (2)

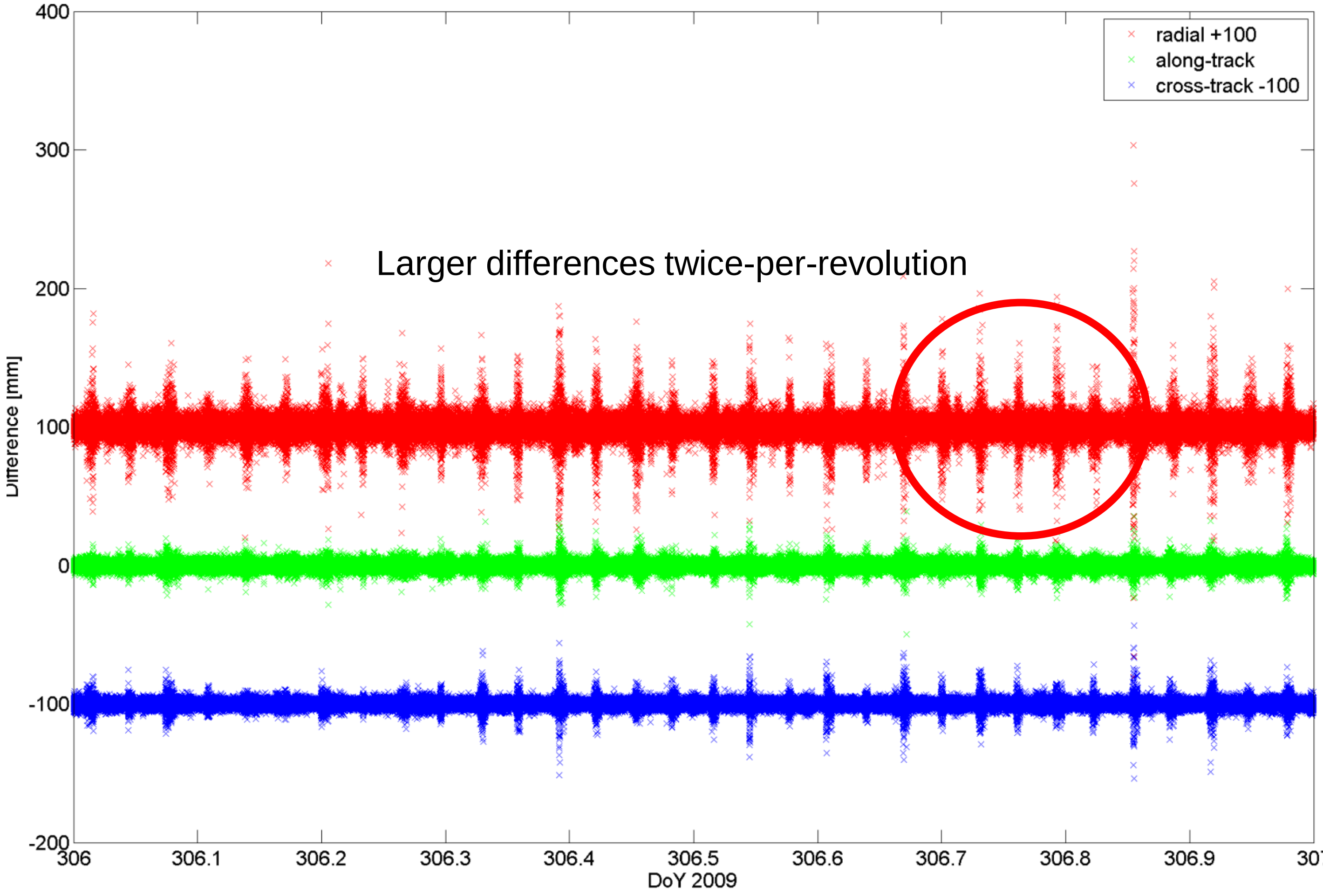

Orbit Differences KIN-RD on 2 Nov, 2009 (3)

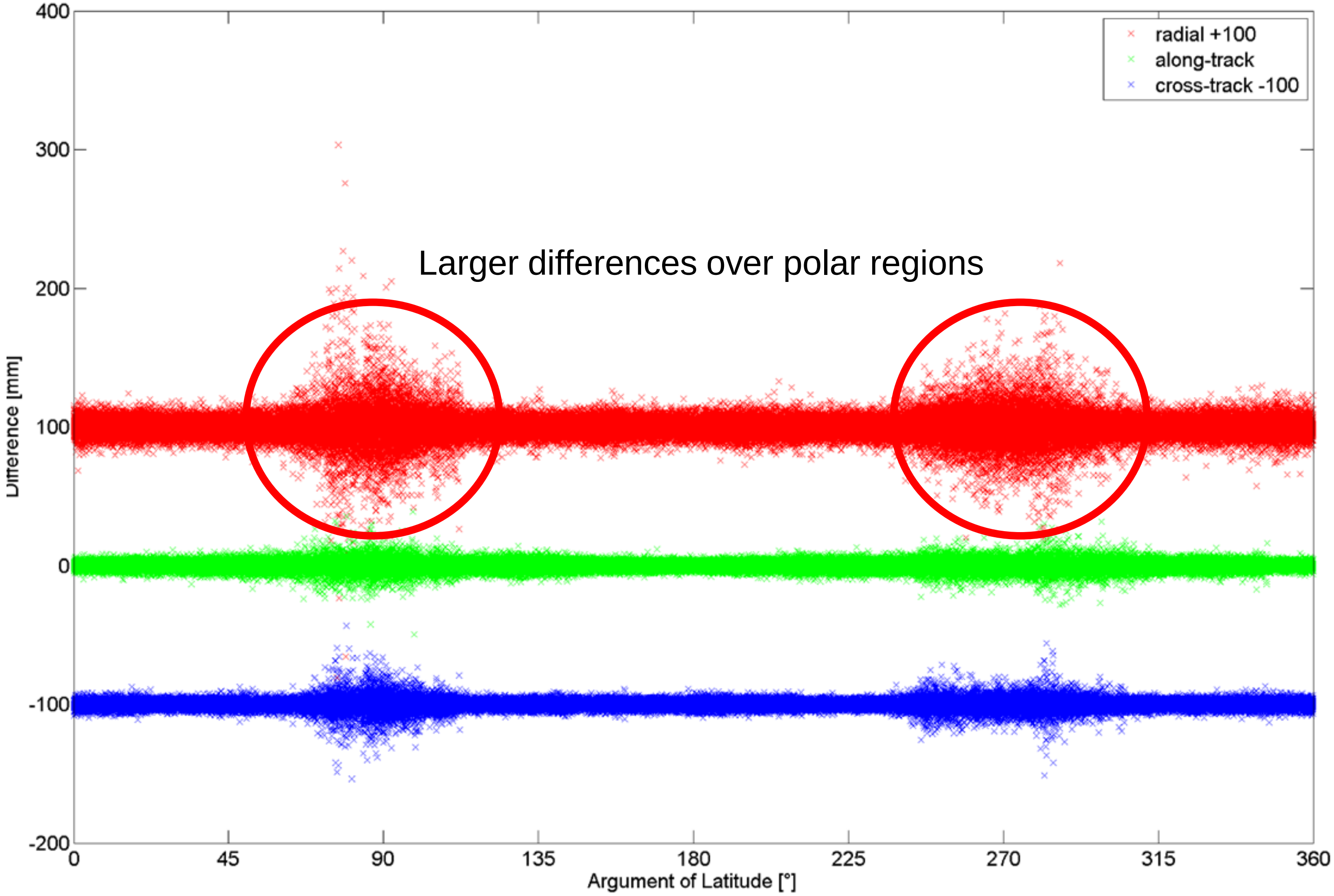

Orbit Differences KIN-RD (1)

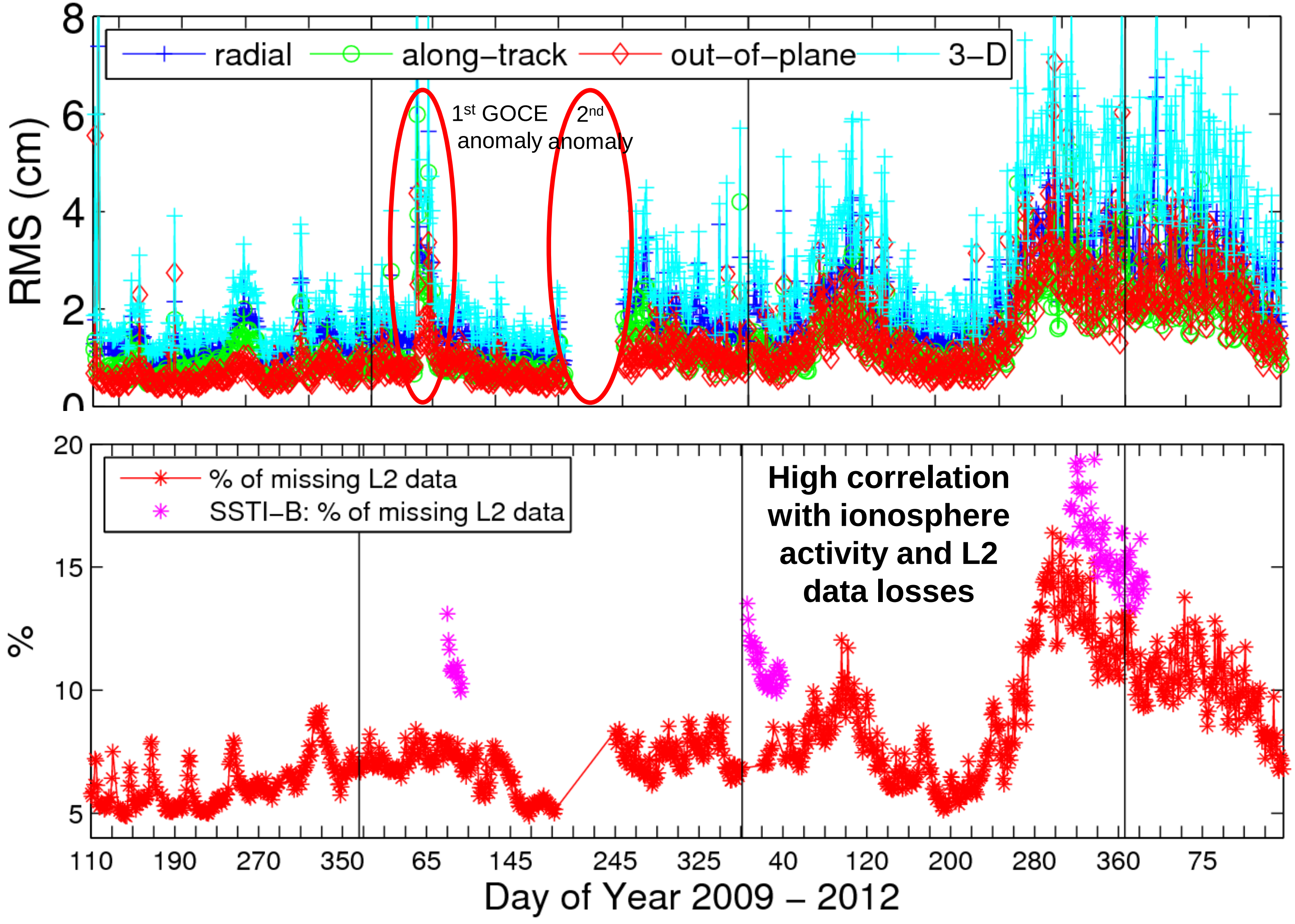

Orbit Differences KIN-RD (2)

Ascending arcs (RMS)

Descending arcs (RMS)

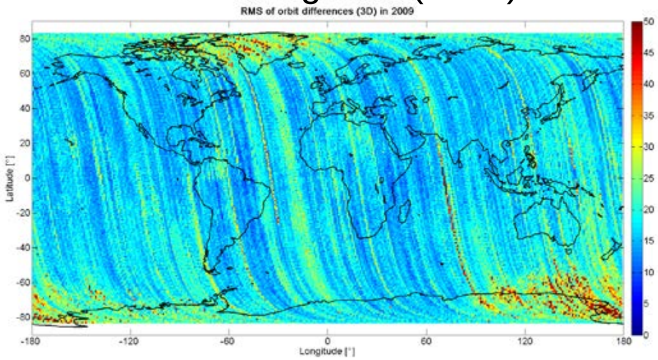

2009

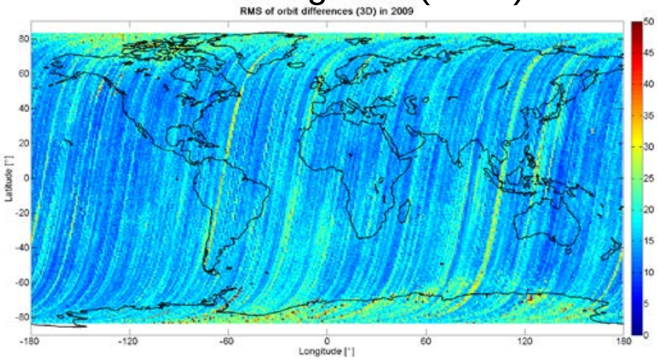

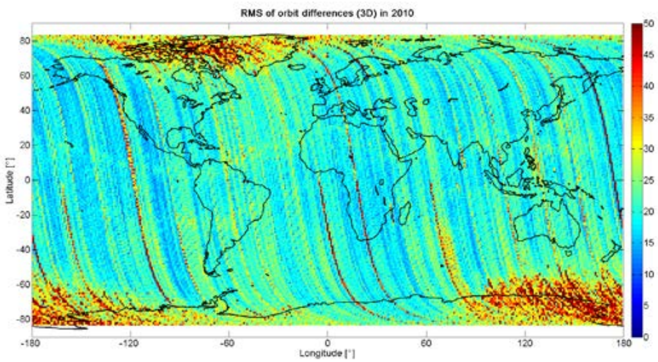

2010

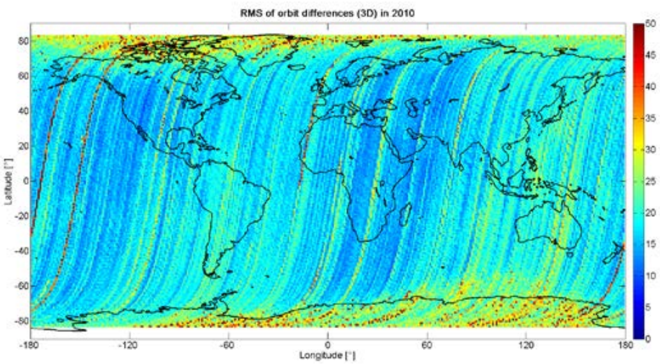

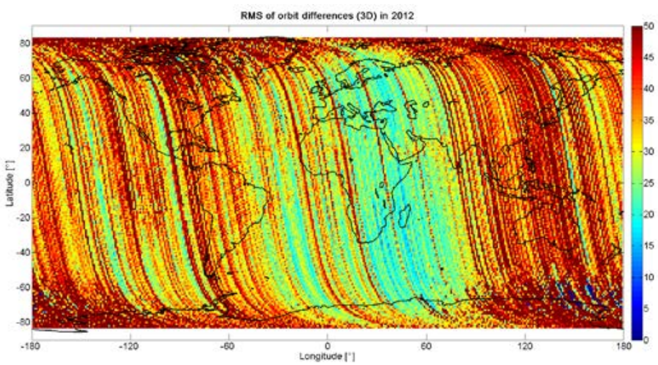

2012

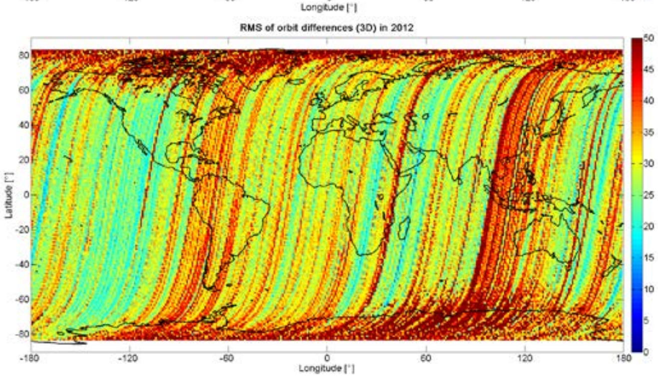

Orbit Differences KIN-RD (3)

Ascending arcs (mean)

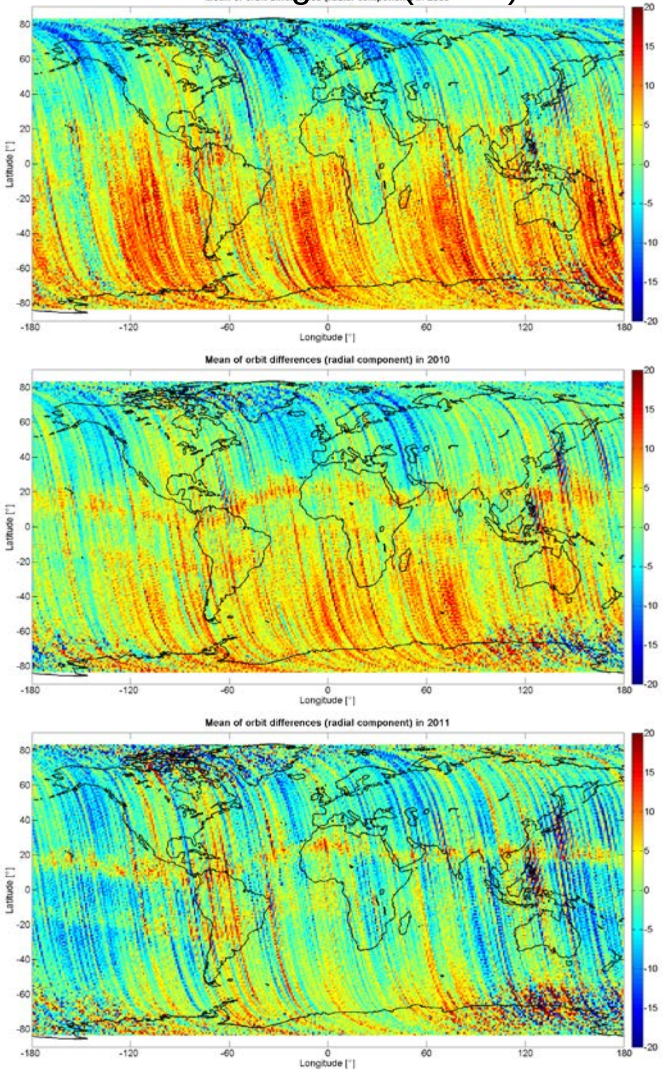

Descending arcs (mean)

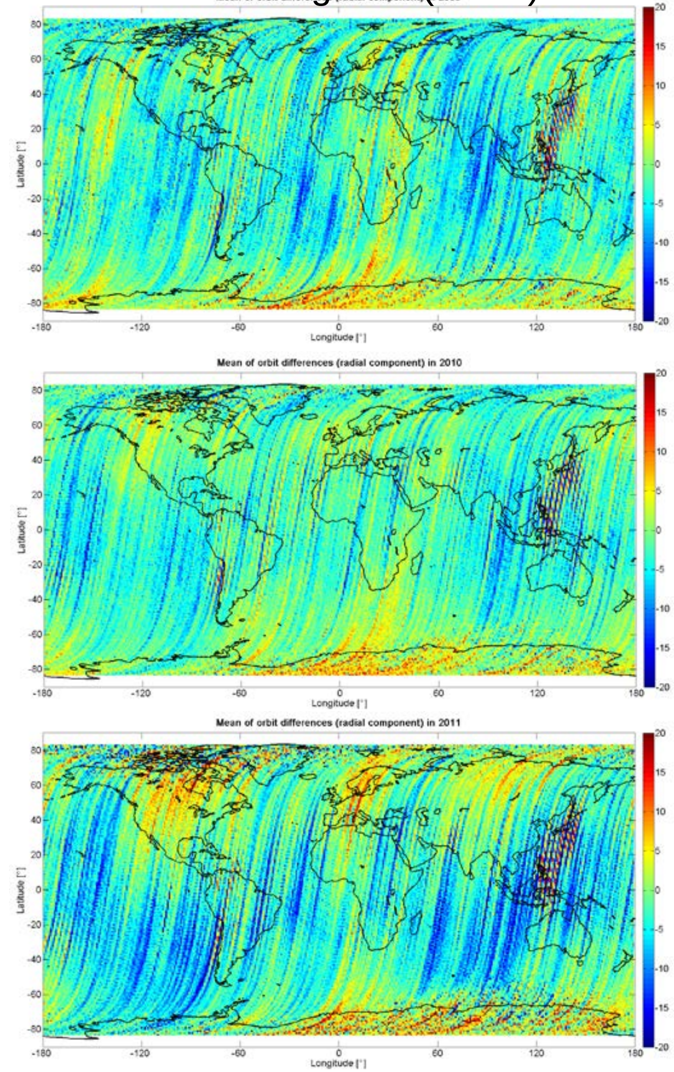

2009

2010

2011

Phase Residuals

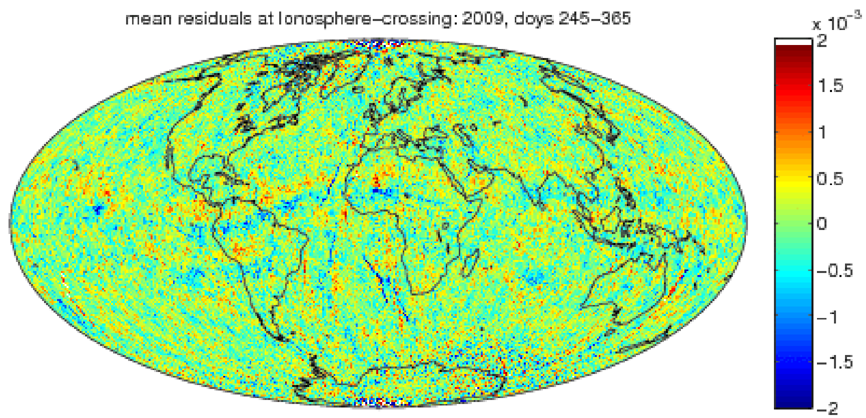

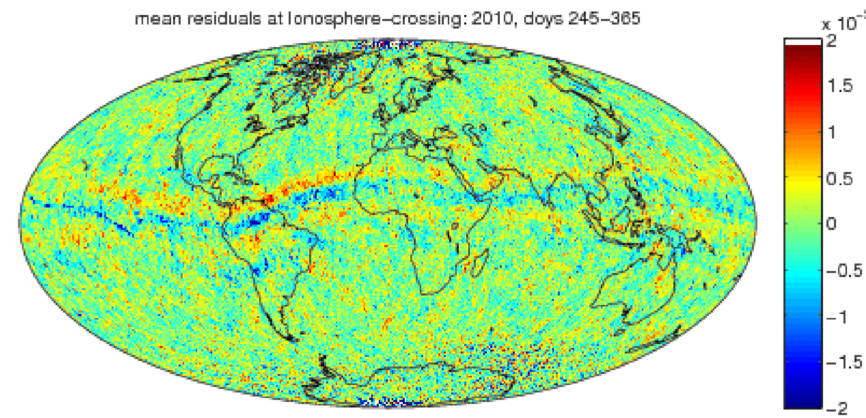

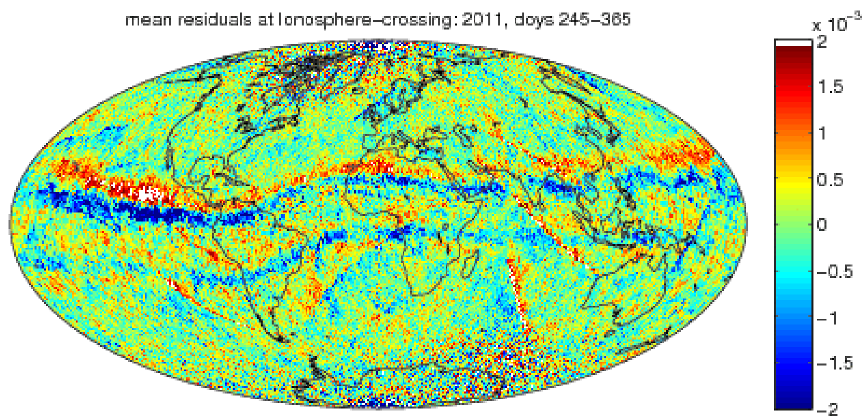

Phase observation residuals mapped to the crossing of the ionosphere layer

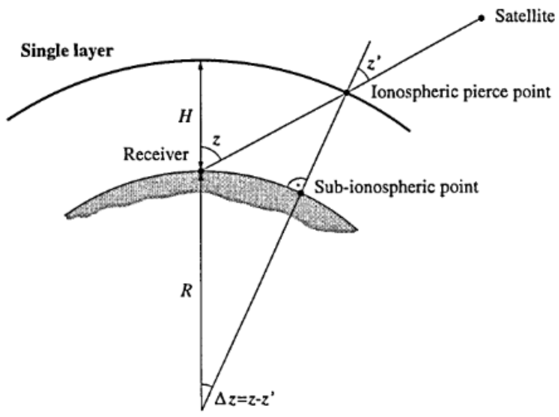

Impact on Gravity Field Solutions

Nov/Dec 2009

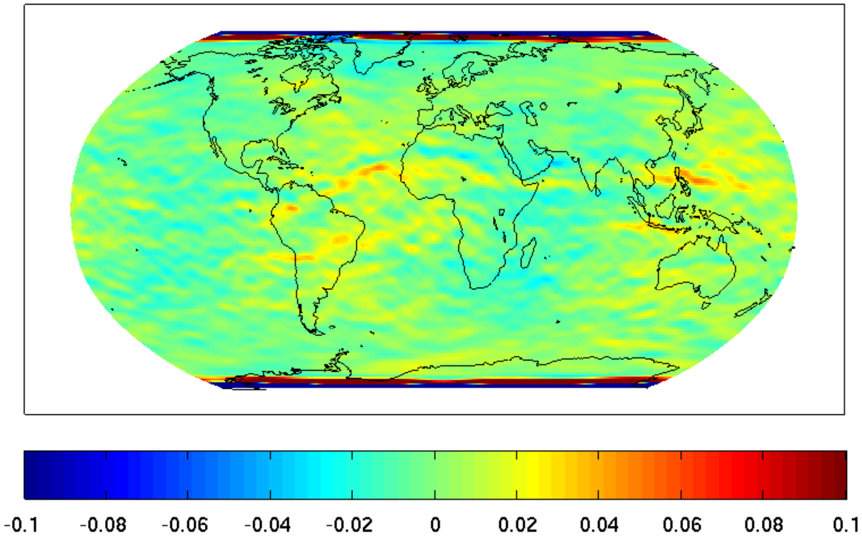

Nov/Dec 2011

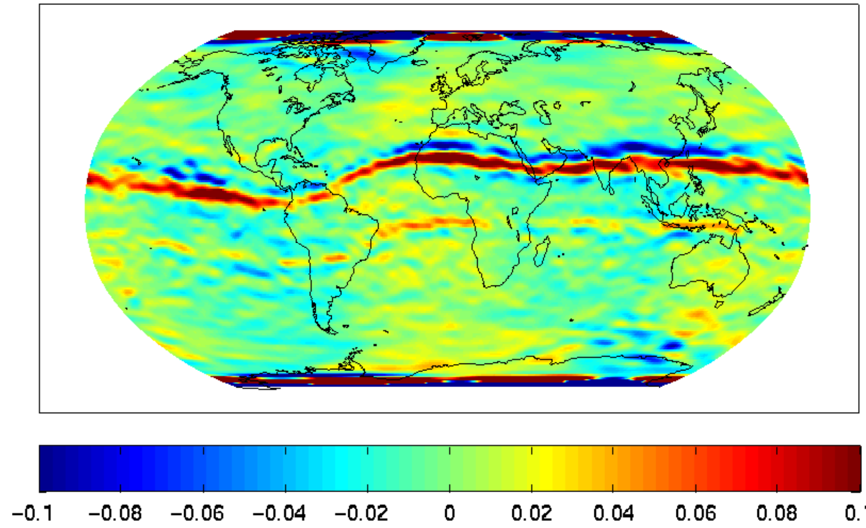

The systematic effect in the phase observation residuals maps into the GOCE GPS-only gravity field solutions achieved so far (Jäggi et al., 2011) …

Literature (1)

Blewitt, G. (1997): Basics of the GPS Technique: Observation Equations, in *Geodetic Applications of GPS*, Swedish Land Survey, pp. 10-54, available at http://www.nbmg.unr.edu/staff/pdfs/Blewitt Basics of gps.pdf

Bigazzi, A., B. Frommknecht (2010): Note on GOCE instruments positioning, XGCE-GSEG-EOPG-TN-09-0007, Issue 3.1, European Space Agency, available at http://earth.esa.int/download/goce/GOCE-LRR-GPS-positioning-Memo_3.1_[XGCE-GSEG-EOPG-TN-09-0007 20v3.1].pdf

Bock, H., R. Dach, Y. Yoon, O. Montenbruck (2009a): GPS Clock Correction Estimation for Near Real-time Orbit Determination Applications. *Aerospace Science and Technology*, 13(7), 415-422, doi: 10.1016/j.ast.2009.08.003

Bock, H., A. Jäggi, R. Dach, G. Beutler, S. Schaer (2009b): GPS single-frequency orbit determination for Low Earth Orbiting satellites. *Advances in Space Research*, 43(5), 783-791, doi: 10.1016/j.asr.2008.12.003

Bock, H., R. Dach, A. Jäggi, G. Beutler (2009c): High-rate GPS clock corrections from CODE: Support of 1 Hz applications. *Journal of Geodesy*, 83(11), 1083-1094, doi: 10.1007/s00190-009-0326-1

Literature (2)

Bock, H., A. Jäggi, U. Meyer, P. Visser, J. van den IJssel, T. van Helleputte, M. Heinze, U. Hugentobler (2011): GPS-derived orbits for the GOCE satellite. *Journal of Geodesy*, 85(11), 807-818, doi: 10.1007/s00190-011-0484-9

Dach, R., E. Brockmann, S. Schaer, G. Beutler, M. Meindl, L. Prange, H. Bock, A. Jäggi, L. Ostini (2009): GNSS processing at CODE: status report, *Journal of Geodesy*, 83(3-4), 353-366, doi: 10.1007/s00190-008-0281-2

Hauschild, A., O. Montenbruck (2008): Real-time clock estimation for precise orbit determination of LEO-satellites, ION-GNSS-2008, Savannah

Jäggi, A., U. Hugentobler, G. Beutler (2006): Pseudo-stochastic orbit modeling techniques for low-Earth satellites. *Journal of Geodesy*, 80(1), 47-60, doi: 10.1007/s00190-006-0029-9

Jäggi, A. (2007): Pseudo-Stochastic Orbit Modeling of Low Earth Satellites Using the Global Positioning System. *Geodätisch-geophysikalische Arbeiten in der Schweiz*, 73, Schweizerische Geodätische Kommission, available at http://www.sgc.ethz.ch/sgc-volumes/sgk-73.pdf

Literature (3)

Jäggi, A., H. Bock, R. Pail, H. Goiginger (2008): Highly Reduced-Dynamic Orbits and their Use for Global Gravity Field Recovery: A Simulation Study for GOCE, *Studia Geophysica et Geodaetica*, 52(3), 341-359, doi: 10.1007/s11200-008-0025-z

Jäggi, A., R. Dach, O. Montenbruck, U. Hugentobler, H. Bock, G. Beutler (2009): Phase center modeling for LEO GPS receiver antennas and its impact on precise orbit determination. *Journal of Geodesy*, 83(12), 1145-1162, doi: 10.1007/s00190-009-0333-2

Jäggi, A., H. Bock, L. Prange, U. Meyer, G. Beutler (2011): GPS-only gravity field recovery with GOCE, CHAMP, and GRACE. *Advances in Space Research*, 47(6), 1020-1028, doi: 10.1016/j.asr.2010.11.008.

Montenbruck, O., Y. Andres, H. Bock, T. van Helleputte, J. van den IJssel, M. Loiselet, C. Marquardt, P. Silvestrin, P. Visser, Y. Yoon (2008): Tracking and orbit determination performance of the GRAS instrument on MetOp-A. *GPS Solutions*, 12(4), 289-299, doi: 10.1007/s10291-008-0091-2

Literature (4)

Montenbruck O., A. Hauschild, Y. Andres, A. von Engeln, Ch. Marquardt (2012): (Near-)Real-Time Orbit Determination for GNSS Radio Occultation Processing. *GPS Solutions*, 17(2), 199-209, doi: 10.1007/s10291-012-0271-y

Švehla, D., M. Rothacher (2004): Kinematic Precise Orbit Determination for Gravity Field Determination, in *A Window on the Future of Geodesy*, edited by F. Sanso, pp. 181-188, Springer, doi: 10.1007/b139065

Visser, P., J. van den IJssel, T. van Helleputte, H. Bock, A. Jäggi, G. Beutler, D. Švehla, U. Hugentobler, M. Heinze (2009): Orbit determination for the GOCE satellite, *Advances in Space Research*, 43(5), 760-768, doi: 10.1016/j.asr.2008.09.016.